# Study of Wave Propagation in Damaged Composite Material Laminates

Ryan J. Lane

Thesis submitted to the Faculty of the
Virginia Polytechnic Institute and State University
in partial fulfillment of the requirements for the degree of

Masters of Science
in
Engineering Mechanics

John C. Duke, Chair
Shima Shahab
Surot Thangjitham

November 6, 2018
Blacksburg, Virginia

Keywords: Wave Propagation, Damaged Composite Laminates, Plate Waves

# Study of Wave Propagation in Damaged Composite Material Laminates

Ryan J. Lane

(ABSTRACT)

The characteristics of carbon fiber composites have enabled these materials to be accepted as replacements for metal parts in industry. However, due to their unsymmetrical material properties, carbon fiber composites are susceptible to damage, such as a delamination, which can cause premature failure in the structure. This has resulted in the need for nondestructive testing methods that can provide quick, reliable results so that these parts can be tested while in service. In this study, an approach was examined that involved a pencil lead break to excite multiple wave modes in a composite plate in an effort to identify key characteristics based on the wavespeed and frequency. These characteristics were then compared to models based on boundary conditions to generate dispersion curves using the transfer matrix method for whole composite plates that were either undamaged or damaged. To first test this approach, experiments were performed on multilayer isotropic plates and then on a composite plate. The results for all cases showed that modes could be excited by the pencil lead break in the undamaged region of the plates that were not theoretical possible in a delaminated region. Also modes that were specific to the delaminated region were excited and this allowed for a clear comparison between the two regions. This approach could be placed into practice to provide routine testing to detect delamination for in-service, carbon fiber composite parts.

# Study of Wave Propagation in Damaged Composite Material Laminates

Ryan J. Lane

(GENERAL AUDIENCE ABSTRACT)

The physical properties of high strength and low weight and the economic benefits of carbon fiber composites has resulted in these materials replacing metals in several industries. It is important, however, to be aware that the change in materials used impacts the different types of damage composites experience compared to conventional metals. One type of damage that could cause a composite part to fail is a delamination or a separation of layers. In order to identify if this damage has occurred, it is beneficial to have an inspection technique that will not damage the part. In this study, a technique was tested that involved breaking a piece of pencil lead on a plate in order to generate multiple wave modes that would propagate in the plate. Based on boundary conditions caused by the damage in the plate, the speed of the wave and frequency content could be compared to an undamaged plate to identify a delamination. A model was created to compare experimental results and demonstrated that using wavespeed and frequency could identify a delamination. The experimental results compared well with the model dispersion curves for a plate with and without a delamination suggesting this approach could be placed into practice to provide routine testing to detect delamination for in-service, carbon fiber composite parts.

# Acknowledgments

I would first like to thank Dr. John C. Duke for giving me the opportunity to join his lab and for providing me guidance throughout the process. I would also like to thank my family: Jim, Carey, Eric, Sara and my dog Ruby. A big thanks to Mac McCord and Danny Reed for helping with specimen fabrication. Lastly, I would like to thank all my friends that have helped me through my journey.

# Contents

**List of Figures** **vii**

**1 Introduction** **1**

1.0.1 Thesis Organization . . . . . 3

**2 Background and Literature Review** **4**

**3 Transfer Matrix Method** **8**

**4 Isotropic Plates** **13**

4.1 Formulation of Governing Equations for Wave Speeds in Isotropic Plates . . 13

4.2 Dispersion Curves Isotropic Plates . . . . . 14

4.3 Experimental Results for Wave Speeds in an Isotropic Plates . . . . . 19

**5 Laminated Carbon Fiber Reinforced Polymeric Matrix Composite Plate** **37**

5.1 Formulation of Governing Equations for Wave Speeds in Composite Plates . 37

5.2 Experimental Results in Composite Plates . . . . . 40

**6 Conclusion** **54**

**7 Future Work** **55**

**Bibliography** **56**

**Appendices** **61**

**Appendix A Dispersion Curve Code** **62**

A.1 Main Program . . . . . 62

A.2 Stiffness Matrix Program . . . . . 64

A.3 Displacement Ratio Program . . . . . 67

A.4 Transfer Matrix Program . . . . . 68

# List of Figures


2.1 Prefatigue C scan of $[\pm 45|0|90]_s$. . . . . 5

2.2 Post fatigue C scan of $[\pm 45|0|90]_s$ specimen showing a delamination between the 0 and 90 layer. . . . . 5

3.1 Multiple layer system with global coordinate system. . . . . 8

4.1 Dispersion curve for 6061 Aluminum 3.175mm thick. . . . . 15

4.2 Dispersion curve for 4130 Steel 3.175mm thick. . . . . 16

4.3 Dispersion curve for 110 Copper 3.175mm thick. . . . . 17

4.4 Dispersion curves for 110 Copper stacked on top of 6061 Aluminum both layers were 3.175mm thick. . . . . 18

4.5 Dispersion curves for 110 Copper stacked on top of 4130 Steel both layers were 3.175mm thick. . . . . 19

4.6 The 3M 966 adhesive sheet applied to one side of a metal plate with a 2 in by 2 in square. . . . . 20

4.7 Large weights being placed on the two metal sheets in order to evenly bond the two plates together. . . . . 21

4.8 Test setup where a PLB was done 10 cm away from an SE1000 transducer in the undamaged portion of the isotropic plates. . . . . 22

4.9 PLB waveform of the undamaged side of the Copper and Aluminum plates. . 23

4.10 PLB waveform of the embedded delamination side of the Copper and Aluminum plates. . . . . 23

4.11 Wavelet Transform of undamaged Copper/Aluminum waveform at 18.5 microseconds. . . . . 24

4.12 Wavelet Transform of undamaged Copper/Aluminum waveform at 23 microseconds. . . . . 25

4.13 Wavelet Transform of undamaged Copper/Aluminum waveform at 40 microseconds. . . . . 26

4.14 Wavelet Transform of damaged Copper/Aluminum waveform at 28 microseconds. . . . . 28

4.15 Wavelet Transform of damaged Copper/Aluminum waveform at 48 microseconds. . . . . 29

4.16 PLB waveform of the undamaged side of the Copper and Steel plates. . . . . 30

4.17 PLB waveform of the damaged side of the Copper and Steel plates. . . . . 30

4.18 Wavelet Transform of undamaged Copper/Steel waveform at 14 microseconds. 31

4.19 Wavelet Transform of undamaged Copper/Steel waveform at 21 microseconds. 32

4.20 Wavelet Transform of undamaged Copper/Steel waveform at 40 microseconds. 33

4.21 Wavelet Transform of damaged Copper/Steel waveform at 28 microseconds. . 34

4.22 Wavelet Transform of damaged Copper/Steel waveform at 50 microseconds. . 35

5.1 Dispersion Curves for Hexcel T650-F584 with a stacking sequence of $[0_2|90_3|0_2]$. 39

5.2 Dispersion Curves for Hexcel T650-F584 with a stacking sequence of $[0_2]$. . . 40

5.3 The finished $[0_2|90_3|0_2]$ composite with the region outlined by silver sharpie representing the embedded delamination. . . . . 41

5.4 Image of the C scan being performed on the embedded delamination region of the plate. . . . . 42

5.5 C scan image of the undamaged part of the plate. . . . . 42

5.6 C scan image of the embedded damage part of the part. . . . . 42

5.7 Composite Test Setup for perform PLBs 10 cm apart and collected the waveforms. . . . . 43

5.8 PLB waveform collected from the undamaged side of the composite plate. . . 44

5.9 PLB waveform collected from the embedded delamination side of the composite plate. . . . . 44

5.10 FFT of undamaged composite PLB waveform. . . . . 45

5.11 FFT of damaged composite PLB waveform. . . . . 46

5.12 Wavelet Transform of the extensional part of the undamaged waveform frequency spectrum at 14 microseconds. . . . . 47

5.13 Wavelet Transform of the extensional part of the undamaged waveform frequency spectrum at 28 microseconds. . . . . 48

5.14 Wavelet Transform of the extensional part of the undamaged waveform frequency spectrum at 11 microseconds. . . . . 49

5.15 Wavelet Transform of the arrival of flexural part of the undamaged waveform frequency spectrum at 61 microseconds. . . . . 51

5.16 Wavelet Transform of the arrival of flexural part of the damaged waveform frequency spectrum at 59 microseconds. . . . . 52

# Chapter 1

# Introduction

Carbon fiber epoxy resin composites have quickly become utilized as replacement material for metal parts. These composites are characterized by their lightweight, strength, and ease of part production. This has resulted in these materials being placed on the fast track for use as mechanical components in such areas as the transportation industry. However, because they are not isotropic in terms of physical and material properties, composites are subject to damage that does not regularly occur in traditionally used metal alloys such as steel and aluminum. Procedures are therefore necessary to assist in detecting the presence of damage in composites. If key characteristics of certain damage features can be derived using governing equations of wave propagation in solids and then identified experimentally, this could greatly improve inspection of carbon fiber composite structures and consequently speed up and improve inspection techniques in industry.

Simple mechanical tests using various strength tests can be used to determine if a part is damaged. If the item being examined fails well below the calculated load or strain point, then there was some type of defect in the part that contributed to the early failure. However, because of the procedures used, after the mechanical test the part would be rendered useless. The need to be able to test a part that does not cause damage has led to the field of Nondestructive Evaluation (NDE). NDE allows the non-invasive evaluation of a part for abnormalities while it is in service. After evaluation, if the part is deemed within acceptable

standards it can continue to be used. Following a nondestructive testing path improves both cost and time efficiency. Not every critical part can be mechanically tested because after testing the parts are unusable, but every critical part could be subjected to NDE at some point in the parts service life which could provide assurances that the part has no damage outside an acceptable tolerance.

In this study, an NDE technique of inputting a wide band signal via a pencil lead break in attempt to excite multiple wave modes was used to determine the presence of certain damage features. The governing equations for the modes were derived using the transfer matrix method and the equations were then modified based on boundary conditions to represent damage in a material system. The equations were first derived for single isotropic plates of various metal alloys as the material symmetry reduces complexity of the solution. The governing equations were then derived while the isotropic plates were stacked on top of each other and then rederived if there was a delamination between a layer. For the experimental setup, the metal plates were then adhesively bounded together with one particular area lacking adhesive to mimic a delamination. Using the same method, the governing equations for plate modes for T650-F584 laminated carbon fiber reinforced polymeric matrix composite plate were found. They were also modified to determine if there was a delamination in between certain layers of the composite. A cross ply laminate of $[0_2|90_3|0_2]$ was made with a Teflon sheet inserted from the side to create a delamination in a certain area of the plate. For all the material systems, pencil lead break experiments were performed and several techniques were used to find the frequency and wave speeds of the waves modes in each material system to find different characteristics that could indicate damage.

### 1.0.1 Thesis Organization

The organization of this thesis is as follows. Chapter 2 provides background and literature review for the study. The chapter presents information about Lamb waves in composite plates and characteristics of lamb waves in a delamination region. There is also a presentation of techniques by other investigators and how this present study can improve upon previous techniques. Chapter 3 discusses the methodology used to calculate and plot the dispersion curves for various material systems. Chapter 4 shows the method applied to isotropic plates in order to test the theory on a less computational-heavy example to determine if the process could be applied to composite plates. Chapter 5 demonstrates the approach on a composite plate and a presentation of results.

# Chapter 2

# Background and Literature Review

Carbon fiber epoxy resin composites consist of a carbon fiber in bundles called tows with epoxy resin as the matrix structure. The fibers are usually aligned in a single direction and provide the strength to the material while the matrix material holds the fibers in place. Composites are usually tailored to the loading occurring in a system meaning the fibers are oriented in such a way that give it the best strength for the given situation. A unidirectional composite is one that for every layer the fibers go in the same direction. A cross ply laminate is when the individual layers which have fibers are ordinated always perpendicular to each other, i.e., the first layer is 0 degrees and the second layer is 90 degrees and so on. Composites have the benefit of having a high strength to weight ratio and depending on the properties close to zero thermal expansion coefficient making them ideal for many fields, e.g., the aerospace industry [1,2]

The ability to use carbon fiber epoxy resin composite mechanical parts which are of lower weight and reduced costs has demonstrated the importance of the need to characterize damage in these parts in both a quick and economic fashion [3]. The use of NDE via wave propagation in solids has shown to be both a rapid and cost-effective approach to identifying damage [4]. For example, the use of guided Lamb waves has helped to detect certain damage defects in a material system [4,5,6]. Lamb waves occur in a free plate where the traction forces at the top and bottom of the plate must be zero. The Lamb waves consist

of two propagating modes: the extensional mode and the flexural mode. Depending on the material properties of the system and characteristics of the propagating wave, higher order extensional and flexural modes can propagate through the material system [5]. Damage in material systems can affect the characteristics of waves propagating through the material.

A critical damage feature that needs to be detected and characterized is a delamination. A delamination is defined as a separation of layers in the through thickness direction [1]. The location of a delamination and characterization of it is important as a delamination can be a failure mechanism of composite structures both in the thickness direction and the in-plane fiber direction. A delamination can lead to a reduction of strength in the in-plane fiber direction leading to earlier failure [7]. An example of a delamination caused by fatigue is shown in Figure 2.1 and 2.2 where a normal incidence ultrasound C scan test of the back surface reflection was performed on the composite specimen.

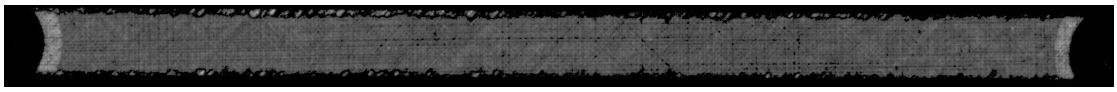

Figure 2.1: Prefatigue C scan of $[\pm 45|0|90]_s$.

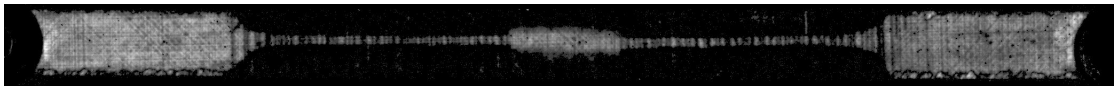

Figure 2.2: Post fatigue C scan of $[\pm 45|0|90]_s$ specimen showing a delamination between the 0 and 90 layer.

The C scan image data is gated in time where the back surface reflection would return to the transducer. In Figure 2.1, the gated captured data returned the whole back surface image except for the edges due to damage caused by cutting the specimens to shape. In contrast, Figure 2.2 shows where a dogbone shape is captured due to the delamination acting as a back surface and returning the waveform earlier than the gated window. This technique is helpful for locating damage in material systems. However, the final product is an image without any mechanical response, and the process is time consuming and requires the part to be either

placed in a water tank or exposed to water. To remove the need for water and improve time efficiency, a pitch/catch scheme using Lamb waves could be used. In this procedure, two elements are in place with one to send a signal into the system at a given frequency and amplitude, and the other to receive some amount of the signal a distance away. For this method to work characteristics of Lamb waves propagating through a delaminated region needed to be identified.

Previous studies have found characteristics of Lamb waves in delaminated regions. Gao and Cawley found that the depth of the delamination affects the amplitude of the first antisymmetric mode and later found that the use of time of flight can help locate the delamination in composite materials [8, 9]. Toyama and Takatsubo used time of flight to identify and determine the size of a delamination caused by impact in composites [10]. Petculescu et al. concluded that a delamination in a composite material affects the arrival time of certain wave modes [11]. Ramadas et al used time of flight of the first antisymmetric mode to determine the size of a delamination in composite material [12]. Yeum found that the first antisymmetric modes time of flight is longer in a delamination [13]. Lastly, Staszewski et al. found that a delamination affects the amplitude of the wave modes traveling through a delamination [14]. These studies therefore indicate that accurately finding and determining the size of a delamination from just a couple of waveforms means that this technique could be used for in service inspection without having to dissemble any components.

A study performed by Shelke et al. used guided Lamb waves in addition to dispersion curves of the material system to detect delamination in aluminum layers. They found that measuring the time of flight of the waves was a promising technique for delamination detection [15]. To detect a delamination in composite plates, Tian et. al. used both Lamb waves and wavenumber analysis and found that the waves trapped in the delamination region demonstrated several of the characteristics reported by previous authors [16]. These studies have

laid the groundwork for the use of guided Lamb waves to excite a particular wave mode to detect damage in both multilayer isotropic metals and composite material systems.

This study provides an alternative approach to previously published work where a particular frequency was inputted in order to excite a certain plate mode. The new approach uses a pencil lead break (PLB) as a wide band signal input in order to excite multiple wave modes. The use of a PLB, also known as Hsu-Nielson source has been established in the nondestructive testing community as a reproducible artificial acoustic emission source [17,18]. For this procedure, a 3mm in length piece of graphite lead is broken at an angle on a specimen to create an acoustic signal in the specimen. A PLB can be used to send a wide band signal into a system and measure wave speed of certain modes at particular frequencies [19]. It can also be used to track wave modes that may not be present when damage is present.

# Chapter 3

# Transfer Matrix Method

In order to validate the results of the experiments used in this study, a dispersion curve for the multiple layer systems was required. The frequency and phase speed pairs for each material system were found using the transfer matrix method (TMM). The TMM was introduced by Thomas and later by Haskell and allows for a signal matrix to be used for multiple layers while satisfying boundary conditions at each layer interface [20, 21]. The technique used in this thesis was refined by Neyfeh, Maghsoodi et al., and Barazanchy et al. to extend from monoclinic layers to transversely isotropic layers to isotropic layers [22,23,24]. As shown in Figure 3.1, a transversely isotropic plate with n stacked layers normal to the $X_3$ in the global axis $(X_1, X_2, X_3)$ where $X_2$ and $X_1$ formed a plane at the top surface of plate where $X_1$ is in the fiber direction. Each layer had a thickness $d_k$ and the total thickness D which was equal to the sum of $d_k$ layers.

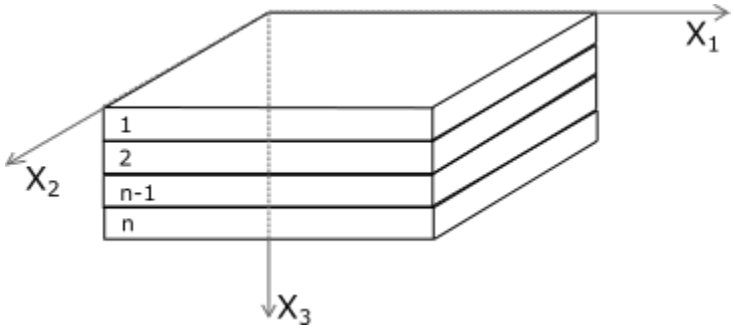


Figure 3.1: Multiple layer system with global coordinate system.

The local coordinate system for each layer was $(x_1, x_2, x_3)$ with $x_1$ in the direction of the fibers

for that particular layer. The momentum equations, linear strain displacement relation, and the constitutive relations for each layer in the cross ply composite are shown in the following equations:

$$\frac{\partial \sigma_{ij}}{\partial x_j} = \rho \frac{\partial^2 u_i}{\partial t^2} \tag{3.1}$$

$$e_{ij} = \frac{1}{2}\left(\frac{\partial u_i}{\partial x_j} + \frac{\partial u_j}{\partial x_i}\right) \tag{3.2}$$

$$\begin{bmatrix} \sigma_{11} \\ \sigma_{22} \\ \sigma_{33} \\ \sigma_{23} \\ \sigma_{13} \\ \sigma_{12} \end{bmatrix} = \begin{bmatrix} C_{11} & C_{12} & C_{12} & 0 & 0 & 0 \\ C_{12} & C_{22} & C_{23} & 0 & 0 & 0 \\ C_{12} & C_{23} & C_{33} & 0 & 0 & 0 \\ 0 & 0 & 0 & C_{44} & 0 & 0 \\ 0 & 0 & 0 & 0 & C_{55} & 0 \\ 0 & 0 & 0 & 0 & 0 & C_{55} \end{bmatrix} \begin{bmatrix} e_{11} \\ e_{22} \\ e_{33} \\ \gamma_{23} \\ \gamma_{13} \\ \gamma_{12} \end{bmatrix} \tag{3.3}$$

A transformation matrix was used to adjust the material values for the rotation of the fiber direction for individual layers. Substitution of the constitutive relations and linear strain displacement equations into the momentum equation resulted in a system of equations in which there were two coupled equations for the P and SV waves and one uncoupled equation for the SH wave shown below:

$$C_{11}\frac{\partial^2 u_1}{\partial x_1^2} + C_{55}\frac{\partial^2 u_1}{\partial x_3^2} + (C_{13} + C_{55})\frac{\partial^2 u_3}{\partial x_1 \partial x_3} = \rho \frac{\partial^2 u_1}{\partial t^2} \tag{3.4}$$

$$C_{66}\frac{\partial^2 u_2}{\partial x_1^2} + C_{44}\frac{\partial^2 u_2}{\partial x_3^2} + = \rho \frac{\partial^2 u_2}{\partial t^2} \tag{3.5}$$

$$C_{33}\frac{\partial^2 u_3}{\partial x_3^2} + C_{55}\frac{\partial^2 u_3}{\partial x_1^2} + (C_{13} + C_{55})\frac{\partial^2 u_1}{\partial x_1 \partial x_3} = \rho \frac{\partial^2 u_3}{\partial t^2} \tag{3.6}$$

Only the P and SV waves were studied. The solutions to these equations were assumed to

be:

$$u_j = U_j e^{ik(x_1+\alpha x_3-ct)} \tag{3.7}$$

Where $U_j$ is the displacement amplitude, k is the wavenumber, $\alpha$ is defined as the ratio of the wave number in the $x_1$ and $x_3$ direction, and c is the phase velocity. The assumed solutions were plugged into the equations 3.4 and 3.6 representing the P and SV waves and the result of which is the matrix below:

$$\begin{bmatrix} C_{11}-\rho c^2+C_{55}\alpha^2 & (C_{13}+C_{55})\alpha \\ (C_{13}+C_{55})\alpha & C_{55}-\rho c^2+C_{33}\alpha^2 \end{bmatrix} \begin{bmatrix} U_1 \\ U_3 \end{bmatrix} = \begin{bmatrix} 0 \\ 0 \end{bmatrix} \tag{3.8}$$

The matrix formed above with the two coupled modes P and SV required the determinant of coefficients set equal to zero such that a nontrivial solution was found. This resulted in a fourth order equation below:

$$A\alpha^4 + B\alpha^2 + C = 0 \tag{3.9}$$

$$A = C_{33}C_{55}$$

$$B = (C_{11}-\rho c^2)C_{33} + (C_{55}-\rho c^2)C_{55} - (C_{13}-C_{55})^2$$

$$C = (C_{11}-\rho c^2)(C_{55}-\rho c^2)$$

The quadratic formula was used to solve the 4th order equation above which resulted in alpha squared pairs such that:

$$\alpha_2 = -\alpha_1, \alpha_4 = -\alpha_3 \tag{3.10}$$

For each $\alpha_j$, $j = 1...4$ the displacement ratios were defined as:

$$W_j = \frac{U_{3j}}{U_{1j}} = \frac{\rho c^2 - C_{11} - C_{55}\alpha_j^2}{(C_{13}+C_{55})\alpha_j} \tag{3.11}$$

$$D_{1j} = (C_{13} + C_{55})\alpha_j W_j \tag{3.12}$$

$$D_{2j} = C_{55}(\alpha_j + W_j) \tag{3.13}$$

Equation 3.11, 3.12, 3.13 and the constitutive relation for the layer Equation 3.3 were used to form a matrix to relate the displacement and stress at the bottom of the plate to the top shown below:

$$\begin{bmatrix} u_{11} \\ u_{22} \\ \sigma_{33} \\ \sigma_{13} \end{bmatrix}_{x_3=d_k} = \begin{bmatrix} T \end{bmatrix} \begin{bmatrix} u_{11} \\ u_{22} \\ \sigma_{33} \\ \sigma_{13} \end{bmatrix}_{x_3=0} \tag{3.14}$$

Where the 4 by 4 matrix for T was defined as:

$$T_1 = \begin{bmatrix} 1 & 1 & 1 & 1 \\ W_1 & -W_1 & W3 & -W_3 \\ D_{11} & D_{11} & D_{13} & D_{13} \\ D_{21} & -D_{21} & D_{23} & -D_{23} \end{bmatrix} \tag{3.15}$$

$$T_2 = diag(e^{ik\alpha_j d_k}) \tag{3.16}$$

$$T = T_1 T_2 T_1^{-1} \tag{3.17}$$

The matrix T is the transfer matrix for one layer. To find the transfer matrix for the whole system, T for each layer was multiplied together as below:

$$T_T = T_n T_{n-1} ... T_1 \tag{3.18}$$

The total transfer matrix for the system was plugged into Equation 3.14 and setting the top and bottom stresses equal to zero to satisfy the traction free boundary conditions indicate

that the determinant of the indices below had to equal zero.

$$Det \begin{bmatrix} T_{31} & T_{32} \\ T_{41} & T_{42} \end{bmatrix} = 0 \tag{3.19}$$

This resulted in an equation where the frequency f and the phase velocity c were variables and finding pairs such that Equation 3.19 was true resulted in the dispersion curves for the material system.

# Chapter 4

# Isotropic Plates

## 4.1 Formulation of Governing Equations for Wave Speeds in Isotropic Plates

It was necessary to first derive the governing equations for isotropic plates prior to demonstrating that using a PLB to excite multiple wave modes in composite materials could track how damage affected the modes. The number of steps when using the transfer matrix method was reduced for the case of isotropic materials due to their symmetry in material properties.

The stiffness matrix for an isotropic material required two independent material properties, the Youngs Modulus (E) and Poissons ratio ($\nu$) which is stated in Equation 4.1:

$$C = \frac{E}{1-\nu-2\nu^2}\begin{bmatrix} 1-\nu & \nu & \nu & 0 & 0 & 0 \\ \nu & 1-\nu & \nu & 0 & 0 & 0 \\ \nu & \nu & 1-\nu & 0 & 0 & 0 \\ 0 & 0 & 0 & 1-2\nu & 0 & 0 \\ 0 & 0 & 0 & 0 & 1-2\nu & 0 \\ 0 & 0 & 0 & 0 & 0 & 1-2\nu \end{bmatrix} \tag{4.1}$$

As described in Section 3 (Transfer Matrix), the stiffness matrix values were plugged into

Equation 3.8 which represents the P and SV wave modes and the determinant of matrix results in Equation 3.9. The solution to the fourth ordered equation is alpha squared pairs found in Equation 4.2

$$\alpha^2 = \frac{\rho v^2 - C_{11}}{C_{11}}, \frac{\rho v^2 - C_{55}}{C_{55}} \tag{4.2}$$

The alpha squared pairs were plugged into the displacement ratios Equations 3.9-3.11. The transfer matrix for each layer was found using Equations 3.15-3.17. If the materials were then stacked, the total transfer matrix was found using Equation 16 which was dependent on the stacking sequence. The dispersion relation was found by applying the stress-free boundary conditions at the top and bottom of the plate as shown in Equation 3.19. Once the dispersion relation was determined the frequency and wave speed pairs were inserted into the equation in order to make the determinate equal to zero. When these pairs satisfied the condition they were plotted to obtain dispersion curves.

## 4.2 Dispersion Curves Isotropic Plates

The metal alloys chosen to be studied were 6061 Aluminum, 4130 Steel, and 110 Copper because they were easy to acquire and inexpensive. The Youngs modulus for 6061 Aluminum is 68.9 GPa, 4130 Steel is 205 GPa, and 110 Copper is 117 GPa [25,26,27]. The Poissons ratio for 6061 Aluminum is 0.33, 4130 Steel is 0.29, and 110 Copper is 0.33 [25,26,27]. The process outlined in Section 3.1 was followed in order to obtain the dispersion curve for each individual material and when the materials were stacked on top of each other. The individual layers were first found because if a delamination occurs the region above and below the delamination acts as two individual free plates and the waves modes acting in each two zones would be different.

The first material examined was 6061 Aluminum. The 6061 version of Aluminum is weldable, corrosion resistant, and has a relative high strength [25]. Frequency and wave speed pairs where inputted up to 1 MHz and 10 km/s respectively. When the determinate of dispersion relation equals zero then that frequency wave speed pair is a root to the equation. When all the roots are plotted on a graph of wave speed vs frequency a pattern is found that represents the wave modes. Normally a dispersion curve plot is wave speed vs frequency-thickness but the thickness was an important parameter and was included into the equations. The dispersion plot for 6061 Aluminum is displayed in Figure 4.1.

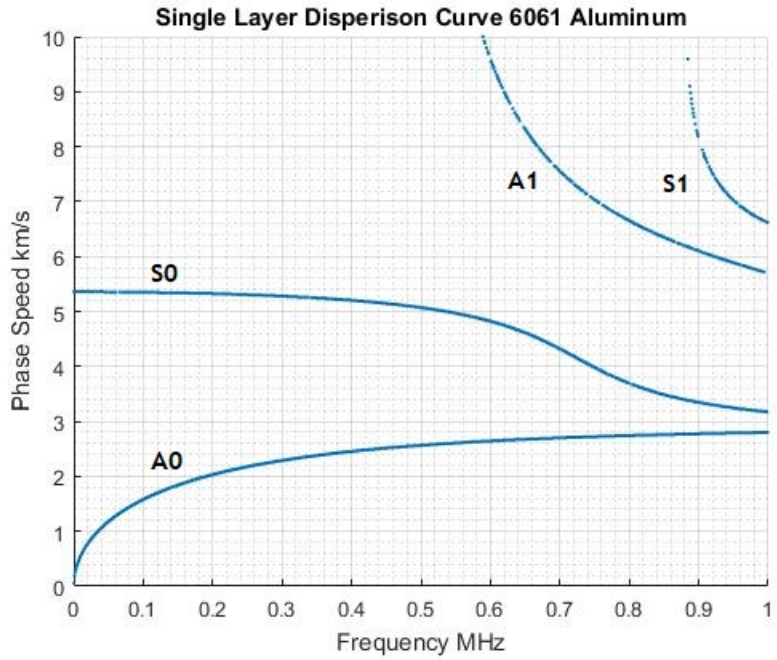


Figure 4.1: Dispersion curve for 6061 Aluminum 3.175mm thick.

There were 4 modes present in the frequency wave speed range plotted. Two were antisymmetric modes labeled A0 and A1 and two were symmetric modes labeled S0 and S1. If the thickness was increased more modes would come into the range.

The next material that was studied was 4130 Steel. 4130 Steel has good strength, weldability, machinability, and atmospheric corrosion resistance [28]. The same steps were followed as

in the Aluminum which resulted in the dispersion curve in Figure 4.2.

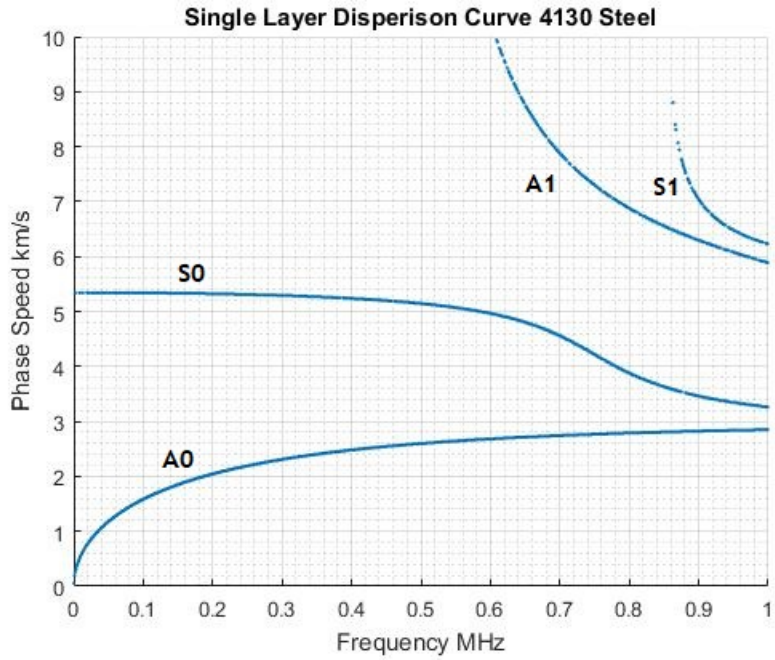


Figure 4.2: Dispersion curve for 4130 Steel 3.175mm thick.

The dispersion curves for the Steel had the same shape as the Aluminum including the same number of modes. There were several wave speed and frequency differences between the two plots. For the steel the quick change in slope that occurred in the first symmetric mode (S0) occurred in the Steel later than the Aluminum. Additionally, there were shifts in the second antisymmetric and symmetric modes (A1, S1) for the Steel compared to the Aluminum.

The last metal alloy that was studied was 110 Copper. 110 Copper is 99.9% Copper and has a high electrical conductivity and is corrosion resist. Copper is well known for its green patina that acts as a protective layer when exposed to the elements. In addition to copper's use in electrical applications it has a high density compared to Aluminum but the same Poissons ratio [29]. The dispersion curves for 110 Copper following the same steps as before are shown in Figure 4.3.

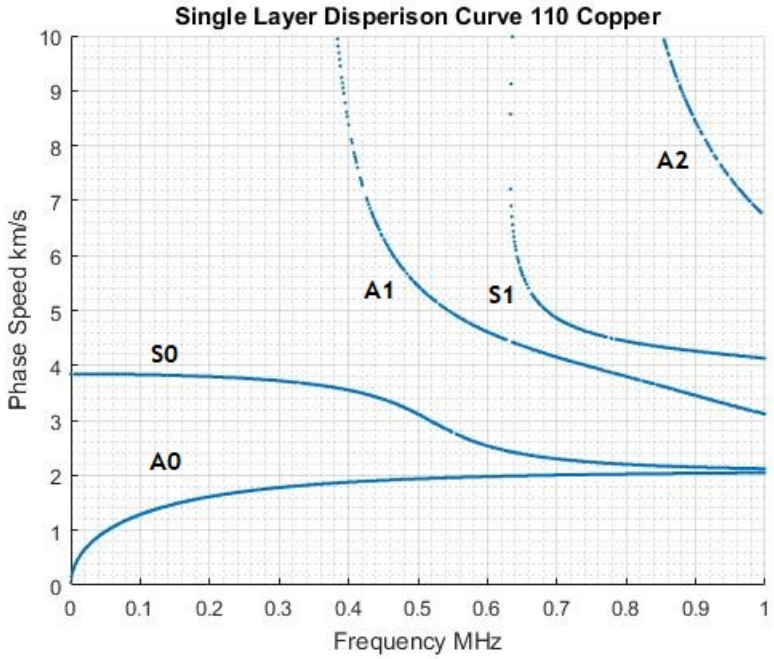


Figure 4.3: Dispersion curve for 110 Copper 3.175mm thick.

Unlike the previous two metals there were 5 modes that appeared in this frequency and wave speed range. Three antisymmetric modes A0, A1, and A2 and two symmetric modes S0 and S1. The shape of the curves was also different which could be helpful in identification when compared to the other metals.

Since this study assumes that there was a delamination in a multilayer stack, dispersion curves for several different metal stacking sequences were required to be computed. The first stacking sequence that was chosen was the 110 Copper on the 6061 Aluminum. The same steps as before were used except there was more than one plate so Equation 16 was used to find the transfer matrix for the whole material system. The dispersion curve for the Copper and Aluminum is shown in Figure 4.4.

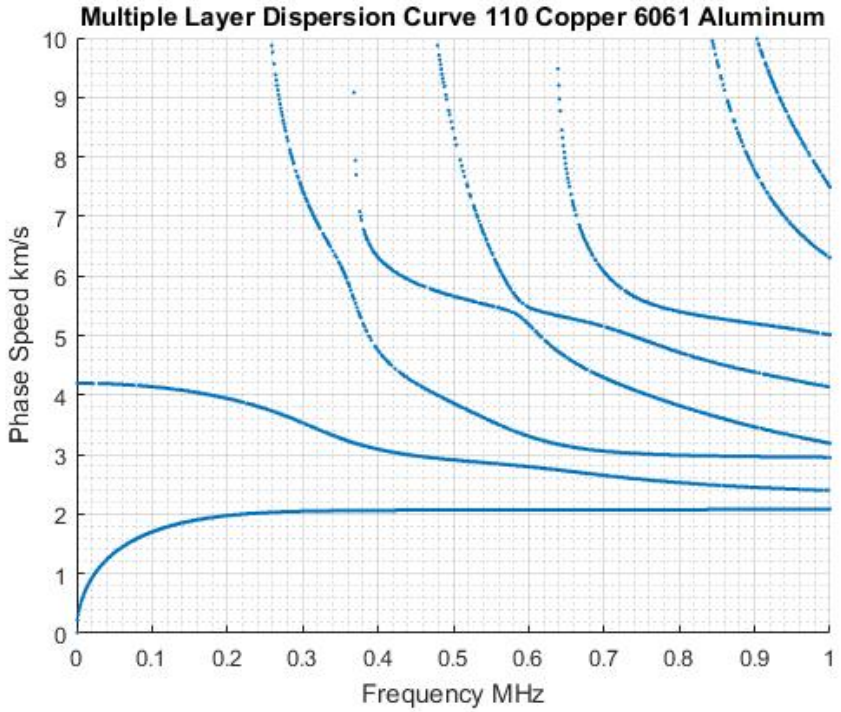


Figure 4.4: Dispersion curves for 110 Copper stacked on top of 6061 Aluminum both layers were 3.175mm thick.

When the materials were stacked on top of each other many more modes were present. This would allow for a PLB to potentially excite all or most of these modes. Following the assumption that a delamination occurs, the area above and below it become free plates or traction free which would allow for a comparison of the single layer dispersion curves to that of the stacked one. This could be used to find characteristics that would define a delamination by the differences in wave speeds and frequencies. The other two metal alloys that were stacked together were 110 Copper and 4130 Steel. The exact steps were followed as for the previous stacked materials. The dispersion curves for Copper and Steel is shown in Figure 4.5.

Similar to the other material stacking sequence this one also had multiple modes enter this frequency and wave speed window. The modes for this stacking sequence were compared to

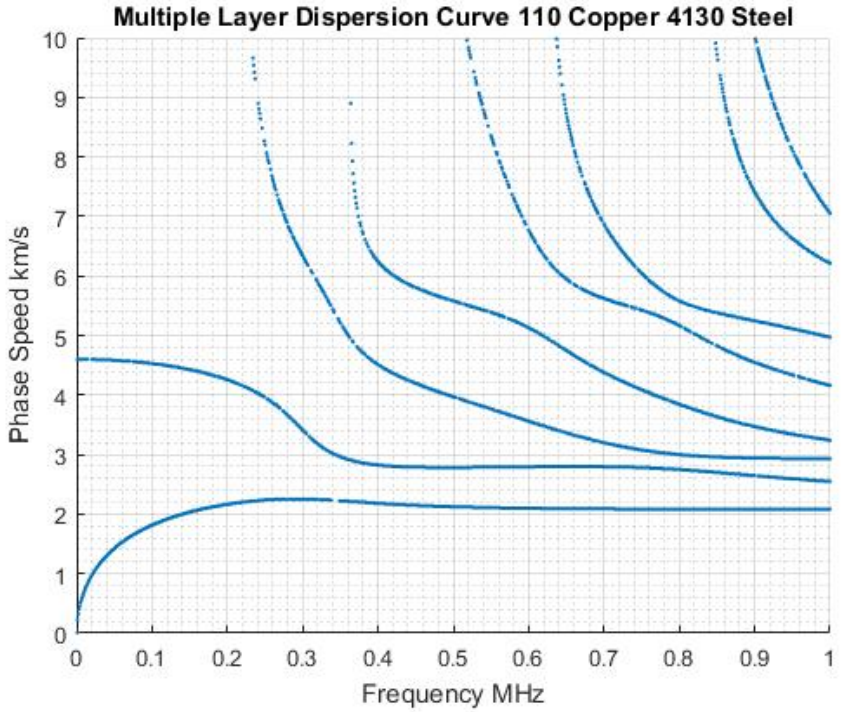


Figure 4.5: Dispersion curves for 110 Copper stacked on top of 4130 Steel both layers were 3.175mm thick.

the modes for each individual layer and there were differences in both frequency and wave speed for both the first two modes in the single layer case and the stacked case. This was a key characteristic because if a PLB is only able to excite the first order modes in both cases then there are key differences that could be used to identify that a delamination has occurred.

## 4.3 Experimental Results for Wave Speeds in an Isotropic Plates

In order to study wave propagation in multiple isotropic plates, the plates needed to be temporarily bonded together. Therefore, 966 3M adhesive sheets were used to bond two of

the metals together. A two-inch by two-inch square was cut in the adhesive sheet to make a makeshift delamination in the layers. A picture of the adhesive sheet is shown in Figure 4.6.

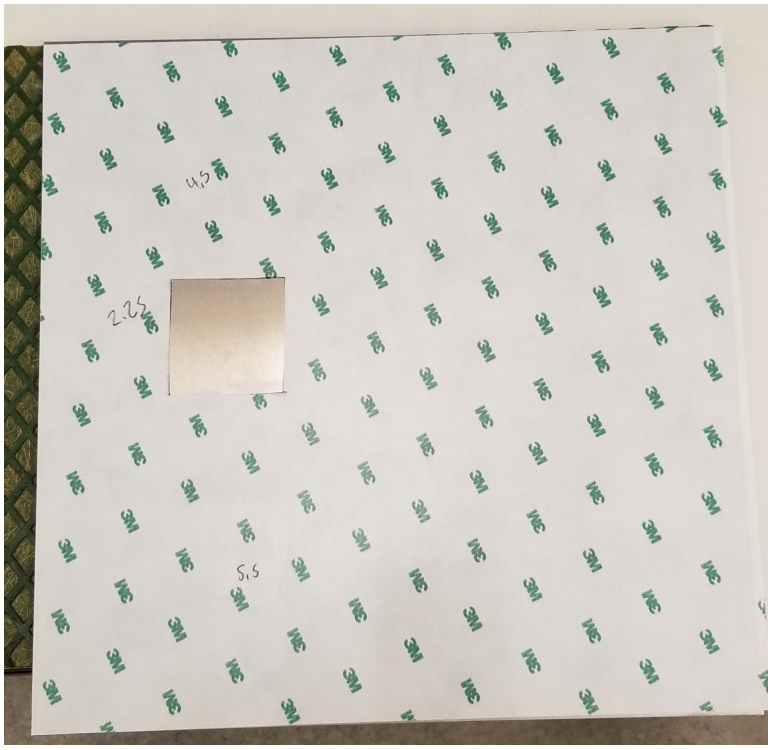

Figure 4.6: The 3M 966 adhesive sheet applied to one side of a metal plate with a 2 in by 2 in square.

After the adhesive sheet was applied to one metal plate the other metal plate was laid on top of it. The metal plates were then placed on a flat counter top. On top of the combined metal plates, a large plate was applied with metal weights placed on top to distribute a large force across the area of the combined plates to ensure large but even pressure. The plates were left with the weights on top for at least 24 hours. A picture of the setup is shown in Figure 4.7.

After 24 hours had passed the weights were removed from the top of the plates. This resulted in the two plates being solidly bonded together. A border was placed around the edge of where the delamination would be in order to be able to collect a waveform in the delaminated

Figure 4.7: Large weights being placed on the two metal sheets in order to evenly bond the two plates together.

region. This setup was done for two material system setups. The first was 110 Copper and 6061 Aluminum and the second was 110 copper and 4130 Steel.

An SE1000 transducer was placed in the center of the delaminated region, and 10 cm away an external trigger was placed where the PLBs would occur. A Picoscope was used to collect the waveforms. The settings for the data acquisition system were 10 Ms/s and 10k samples were collected. This was done for both sides of the plate: the embedded damage side and the undamaged side. A picture of the test setup is shown in Figure 4.8.

In both cases the transducer was placed on top of the copper plate. This was due to the dispersion curves for Copper were different than that of Aluminum and Steel which look similar and may have provided the greatest chance of exciting different modes.

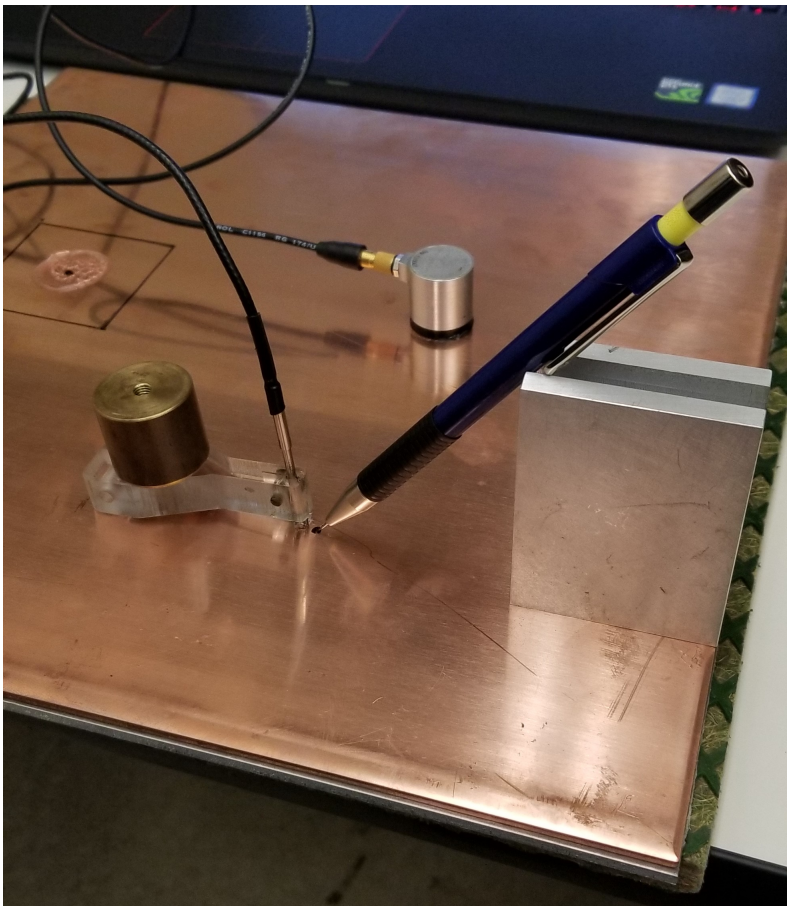

Figure 4.8: Test setup where a PLB was done 10 cm away from an SE1000 transducer in the undamaged portion of the isotropic plates.

A 0.3 mm lead pencil with a piece of lead that was 3mm long was used to perform the PLBs. A total of 3 PLBs were performed at each location on the plates. The 110 Copper and 6061 Aluminum plates were combined and PLBs performed. An example of a waveform collected in in the undamaged region is shown in Figure 4.9 and for the damaged section is shown in Figure 4.10.

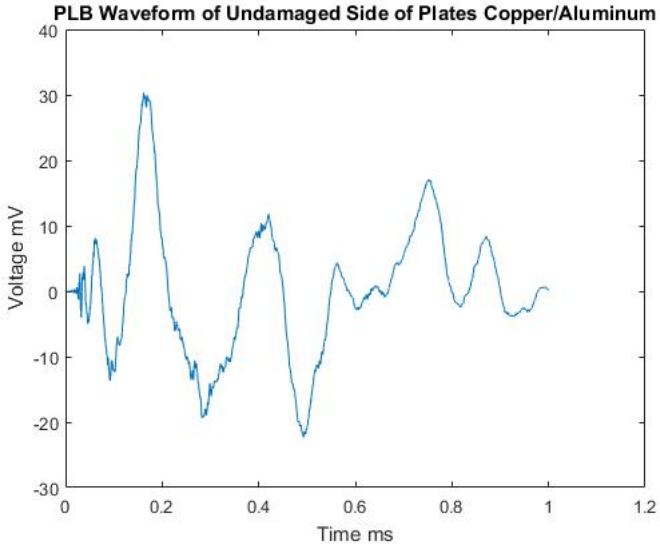


Figure 4.9: PLB waveform of the undamaged side of the Copper and Aluminum plates.

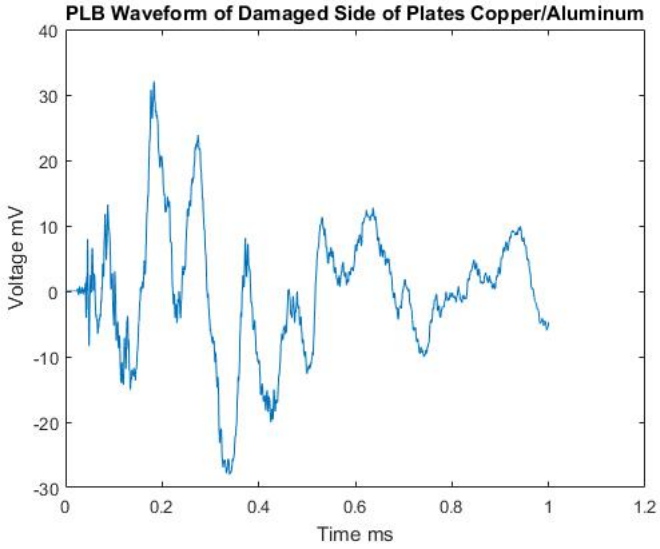


Figure 4.10: PLB waveform of the embedded delamination side of the Copper and Aluminum plates.

The overall shape of the waveforms is different in addition to possibly the arrival times of the extensional parts of the waveforms. In order to see both the arrival times and frequency content of the waveforms a Wavelet Transform was done. A Wavelet transform breaks the waveforms into what is basically an Fast Fourier Transform (FFT) but in time. Vallen Wavelt

Software was used to perform the Wavelet Transformation [30]. The wavelet transform was first done on the extensional part of the undamaged waveform. The result of the transform and frequency spectrum at 18.5 microseconds is shown in Figure 4.11.

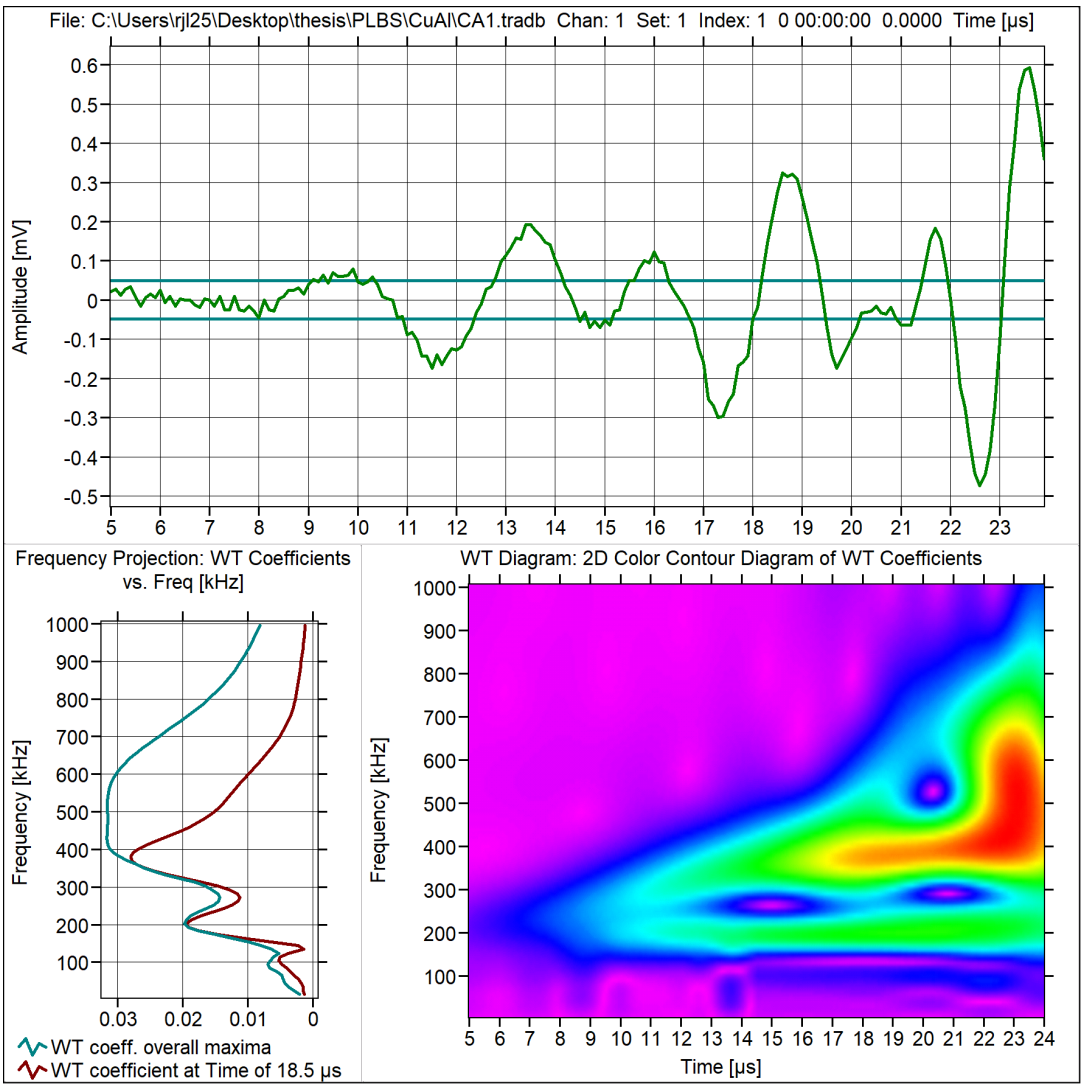


Figure 4.11: Wavelet Transform of undamaged Copper/Aluminum waveform at 18.5 microseconds.

The speed of the wave traveling a distance of 10 cm in 18.5 microseconds was 5.41 km/s. The peak frequency at this point in time were 100 kHz, 200 kHz, and 375 kHz. Referencing Figure 4.4, the dispersion curves for the Copper and Aluminum combined with a wavespeed

of 5.41 km/s and a frequency of 375 kHz corresponded to the higher order mode that starts at 10 km/s and 250 kHz. This mode did not appear in the copper plate when the dispersion curves were calculated. The frequency spectrum was then done at 23 microseconds which is shown in Figure 4.12.

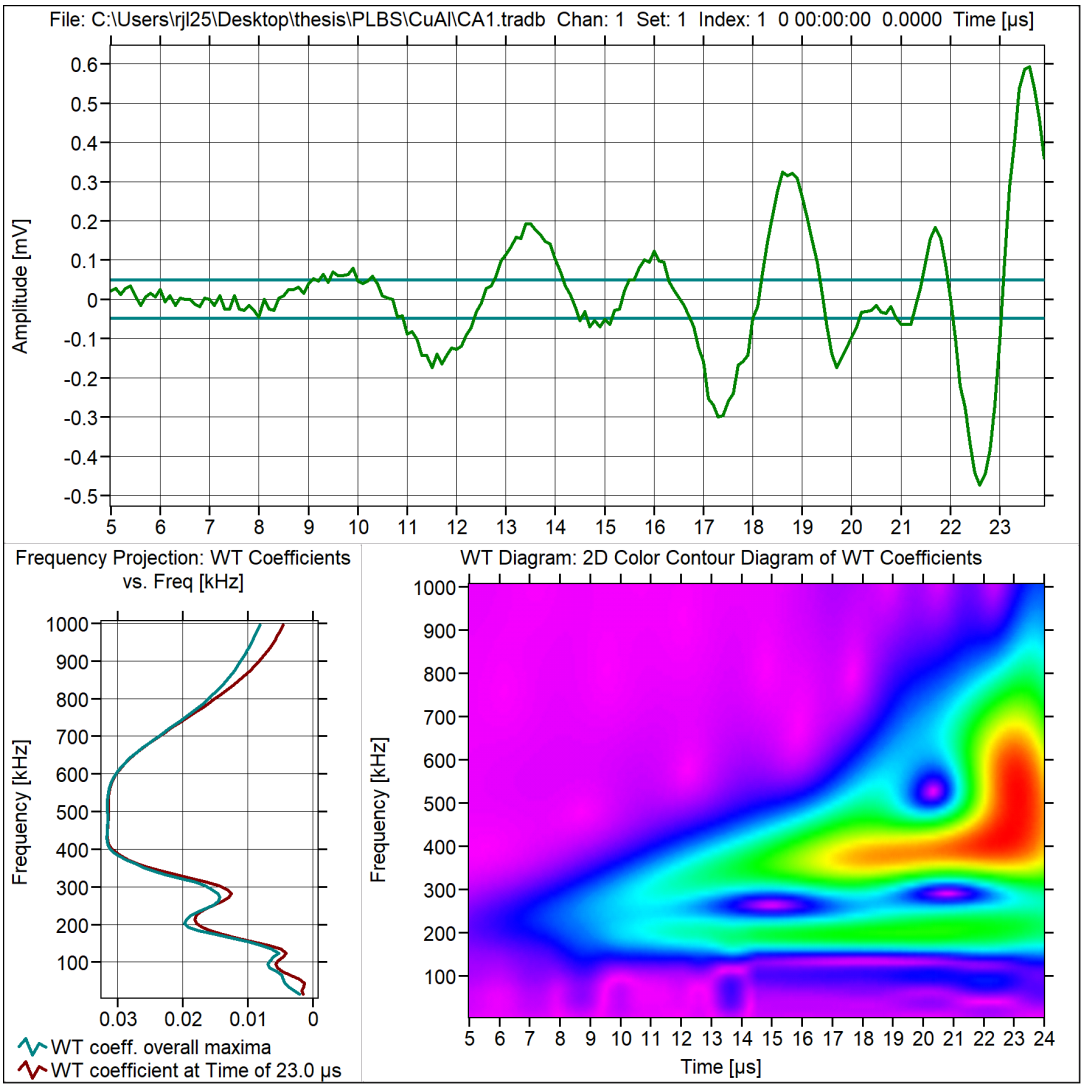


Figure 4.12: Wavelet Transform of undamaged Copper/Aluminum waveform at 23 microseconds.

The speed of the wave at 23 microseconds was 4.35 km/s. The peak frequencies at this point in time were 75 kHz, 225 kHz, and between 400 to 600 kHz. The 75 kHz corresponds to

the mode in Figure 4.4 that starts at 4.3 km/s. The 400 to 600 kHz seems to correspond to several of the higher order moods in that frequency range. Again these higher modes were not present in the signal Copper plate dispersion curves in Figure 4.3. Lastly, for the undamaged waveforms, the arrival of the flexural part had a Wavelet transform performed which is shown in Figure 4.13.

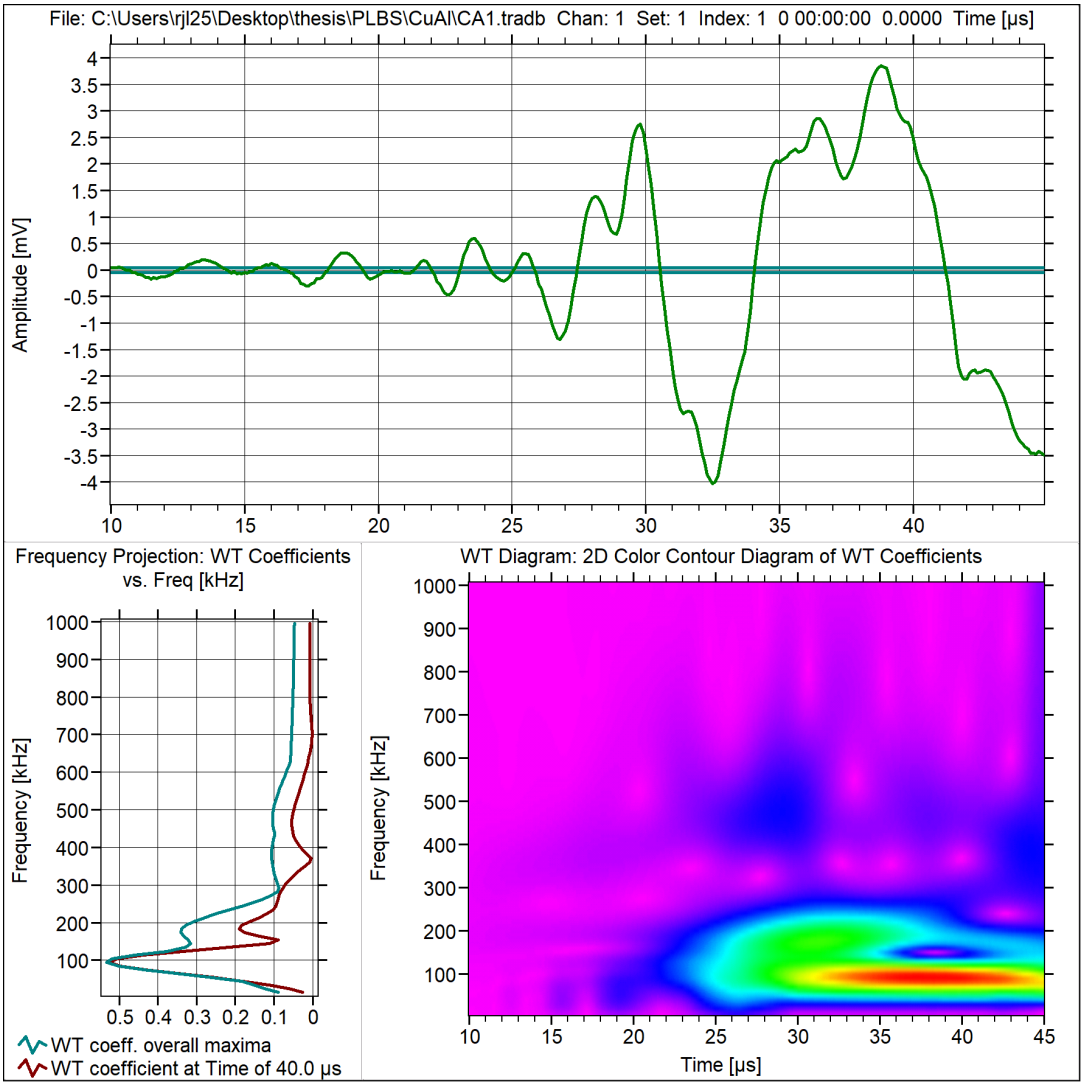


Figure 4.13: Wavelet Transform of undamaged Copper/Aluminum waveform at 40 microseconds.

The speed of the wave at this point in time was 2.00 km/s. With peak frequencies at 100

kHz and 175 kHz. Both these frequencies correspond to lowest mode that starts at 0 km/s in Figure 4.4. The extensional part of the damaged waveform was analyzed next. It can be seen that these waveforms in the damage section were slower and arrive later in time than that of the undamaged waveforms. The arrival time of the undamaged wave was 8 microseconds while the damaged arrival time was 23 microseconds. This also corresponded to the dispersion curves for each case. The results of the Wavelet transformation at 28 microseconds is shown in Figure 4.14.

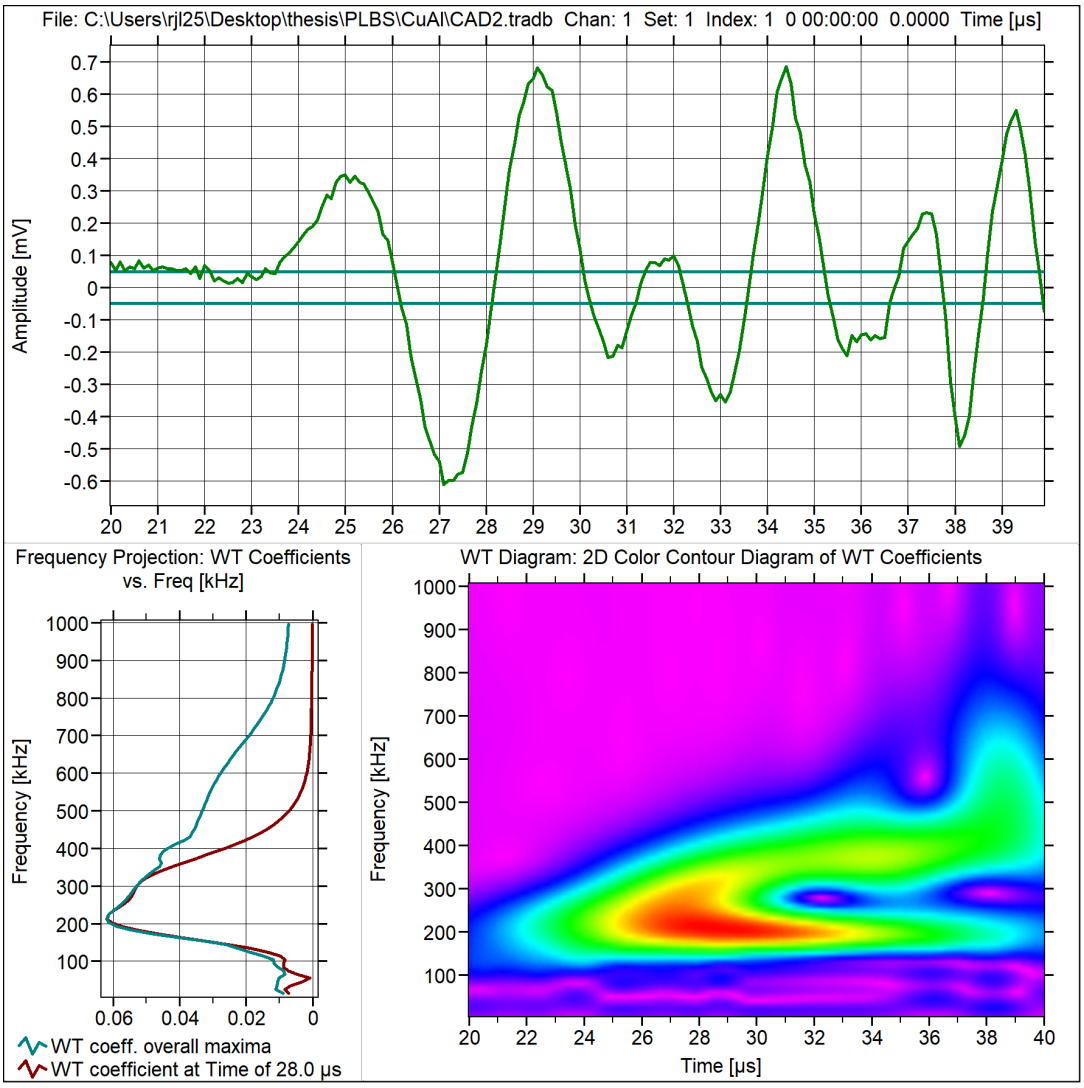


Figure 4.14: Wavelet Transform of damaged Copper/Aluminum waveform at 28 microseconds.

The speed of the wave at 28 microseconds was 3.57 km/s and the peak frequencies were 25 kHz and 215 kHz. Both of these frequencies corresponded to the first symmetric mode labeled as S0 in the Copper plate in Figure 4.3. Lastly, the arrival flexure part of the damaged waveform was analyzed and the results are shown in Figure 4.15.

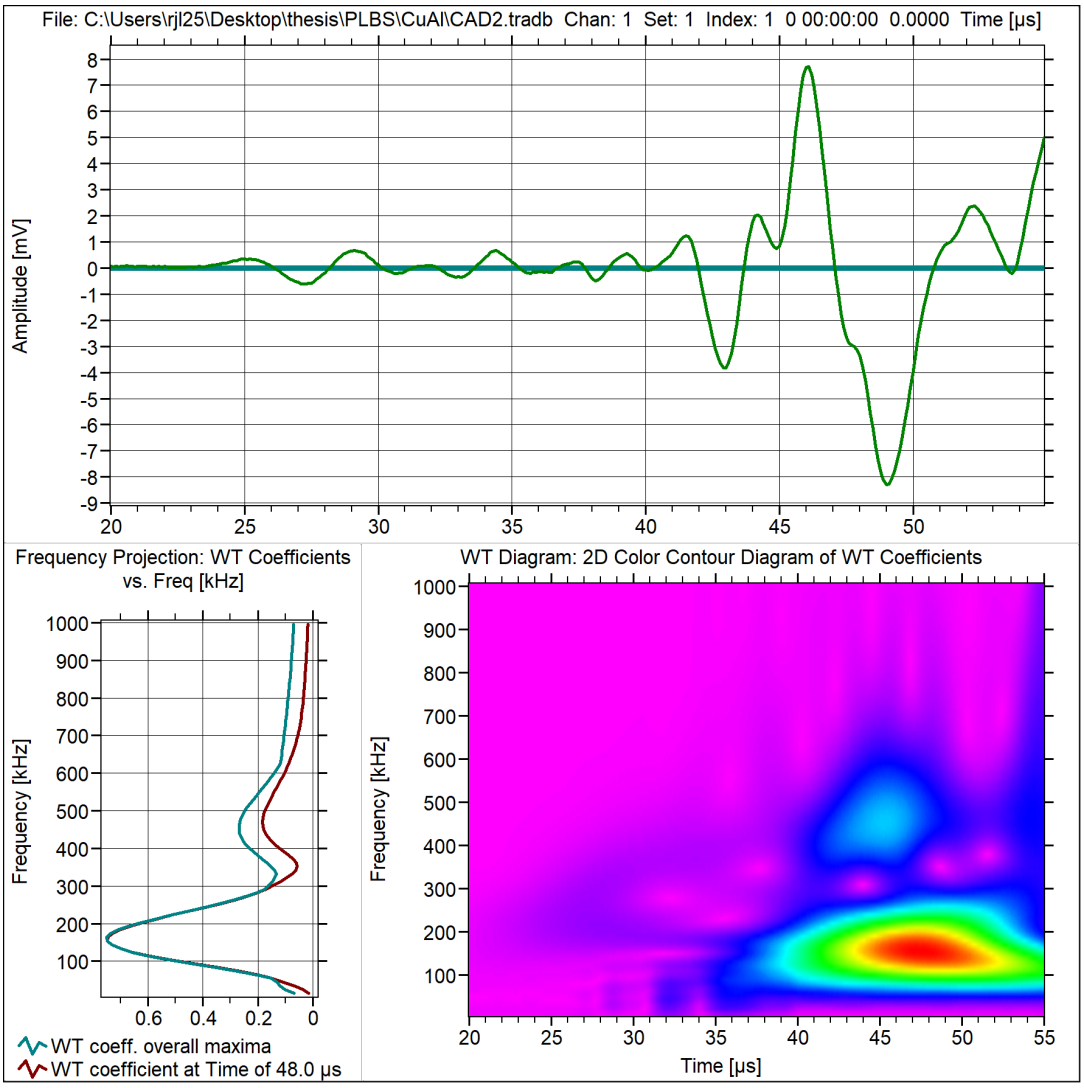


Figure 4.15: Wavelet Transform of damaged Copper/Aluminum waveform at 48 microseconds.

The speed of the wave was 2.08 km/s and with peak frequencies of 150 kHz and 450 kHz. At this wave speed both those frequencies were the first antisymmetric mode in Figure 4.3 labeled as A0.

The next plates that were stack together were the 110 Copper and 4130 Steel. Three PLBs were done on both sides of the plate using the same pencil and setup as before. The collected waveform for the undamaged side of the plate is shown in Figure 4.16.

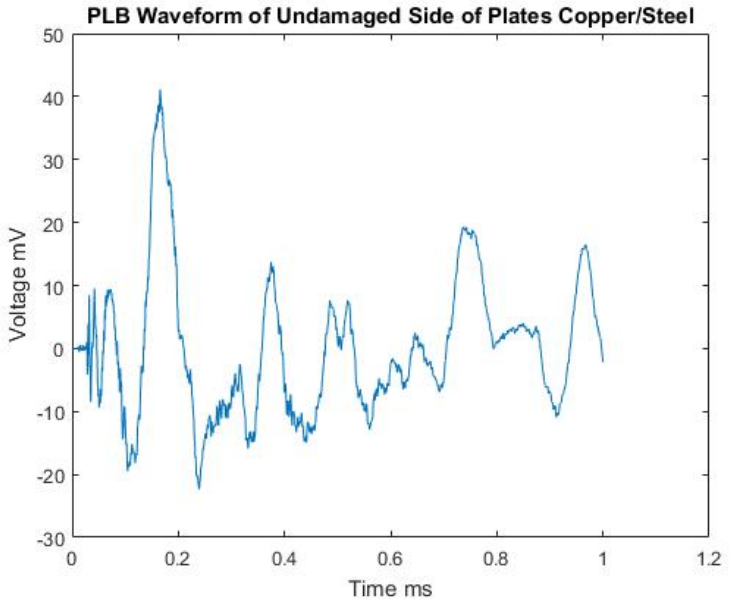


Figure 4.16: PLB waveform of the undamaged side of the Copper and Steel plates.

The collected waveform had a similar shape for this case in the last setup this is most likely due to the fact that the dispersion curves for Steel and Aluminum were similar. The waveform for the embedded delamination is shown in Figure 4.17.

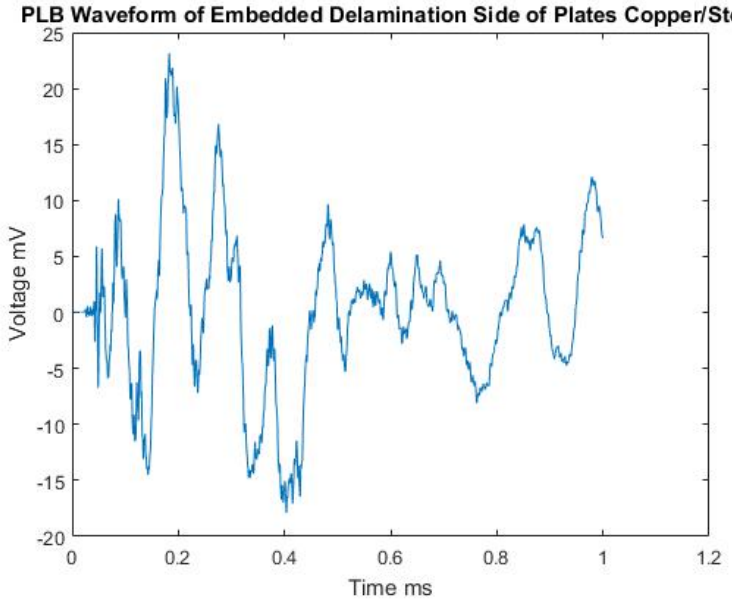


Figure 4.17: PLB waveform of the damaged side of the Copper and Steel plates.

As expected the waveform for the damaged side is similar to that of the pervious case as the transducer was placed on top of the copper plate for both cases. This provided some validity to the process that was being used to create the delamination.

A Wavelet Transform was then performed on the waveforms for this case. The extensional part of the undamaged side was analyzed first. The Wavelet Transformation was performed at 14 microseconds in the undamaged waveform and the results are shown in Figure 4.18.

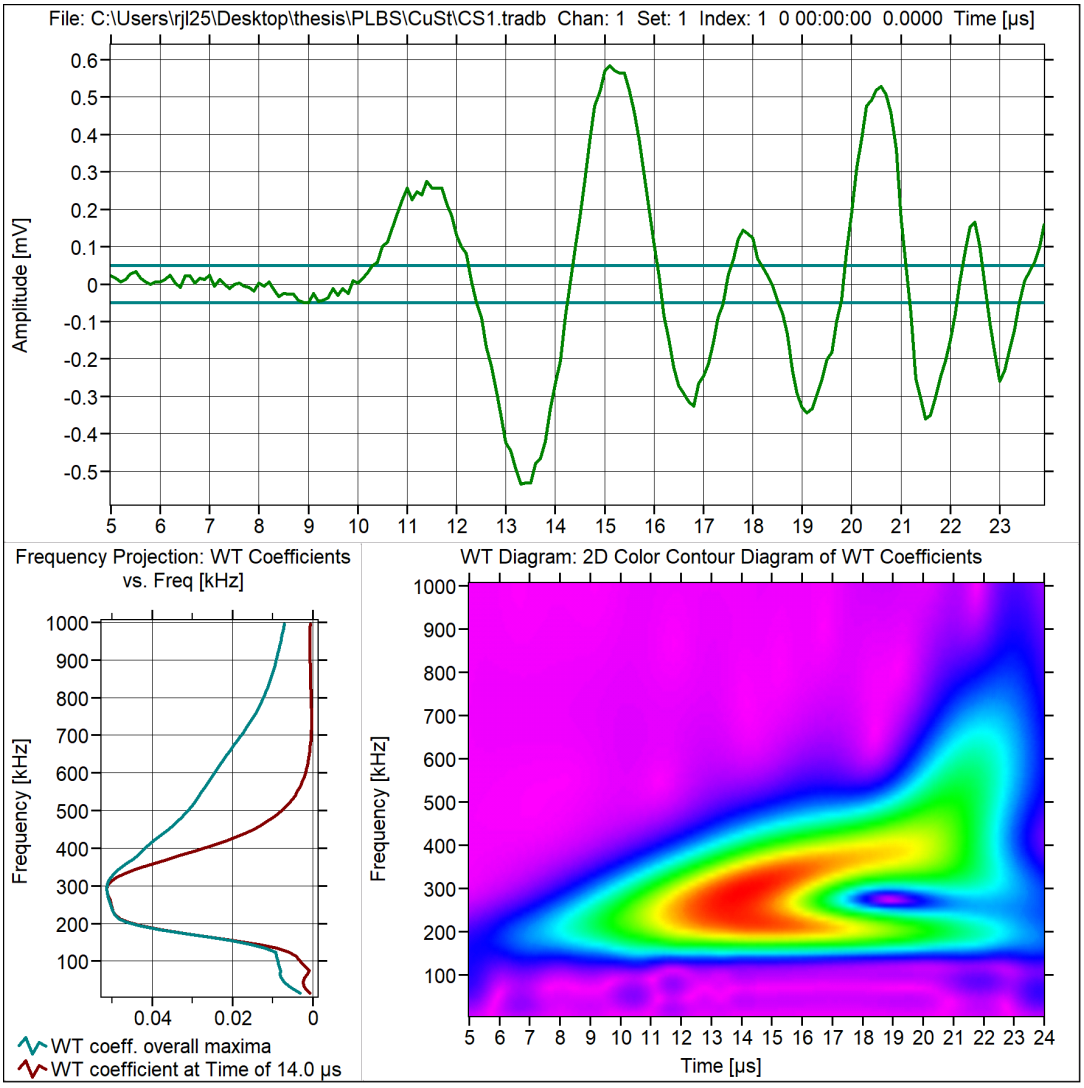


Figure 4.18: Wavelet Transform of undamaged Copper/Steel waveform at 14 microseconds.

The speed of the wave was 7.14 km/s and the peak frequencies were between 200 kHz and 300 kHz. This corresponded to the higher order mode in Figure 4.5 that starts at 10 km/s and 230 kHz. That fact that this mode was excited by the PLB was a good sign because this mode was not possible in the single Copper plate. The results for the Wavelet Transform at 21 seconds are shown in Figure 4.19.

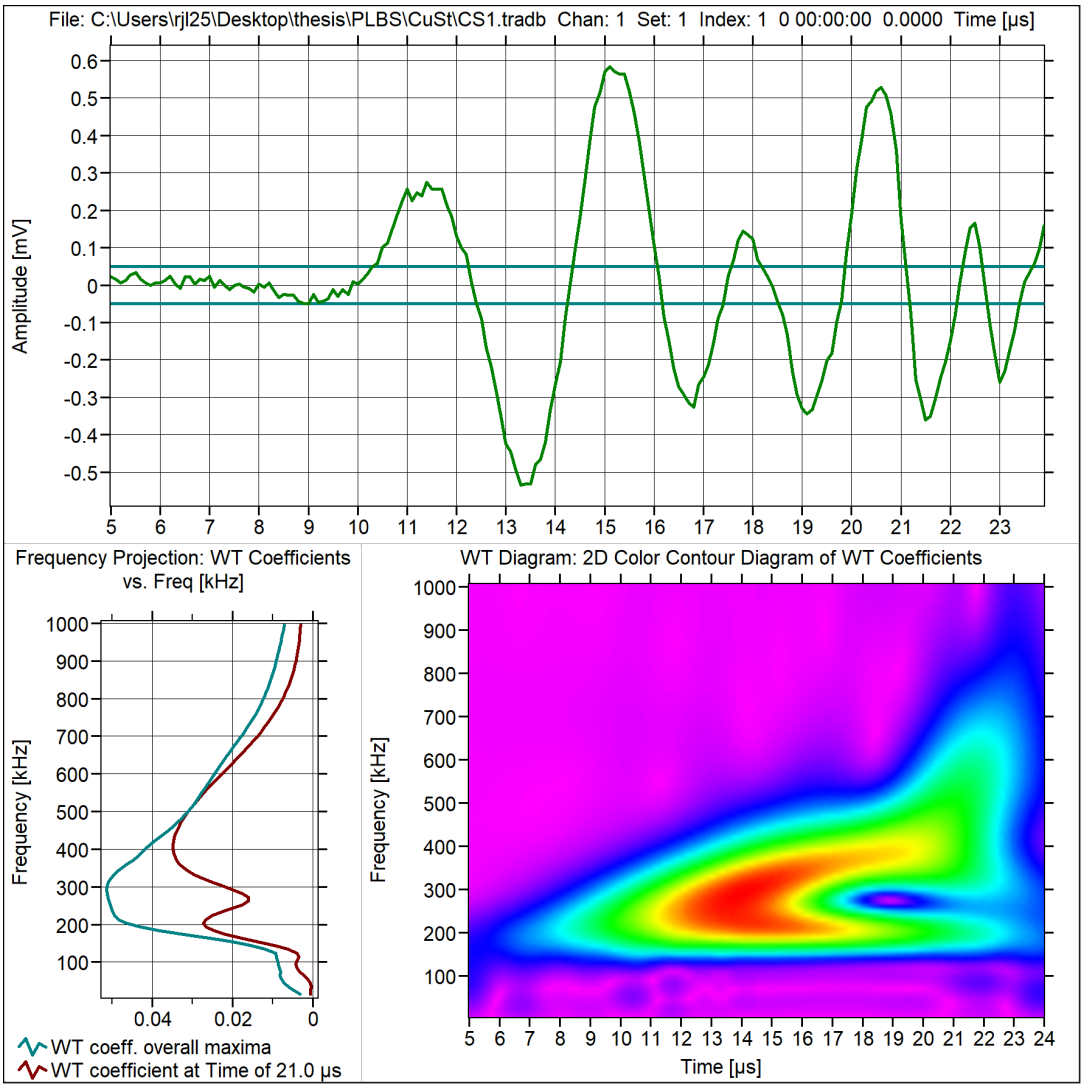


Figure 4.19: Wavelet Transform of undamaged Copper/Steel waveform at 21 microseconds.

The wavespeed at this point in time was 4.76 km/s with peak frequencies of 75 kHz, 200 kHz, and 400 kHz. The 400 kHz corresponds to the higher order mode that was found in

Figure 4.18. The frequencies of 75 kHz and 200 kHz corresponded to the mode that starts at 4.7 km/s in Figure 4.5. This mode, if compared to the S0 mode in Figure 4.3 for the single Copper plate, had a higher wavespeed. The last Wavelet Transform that was done of the undamaged waveform was at 40 microseconds which corresponded to the arrival of flexural part of the waveform. The results of Wavelet transformation can be seen in Figure 4.20.

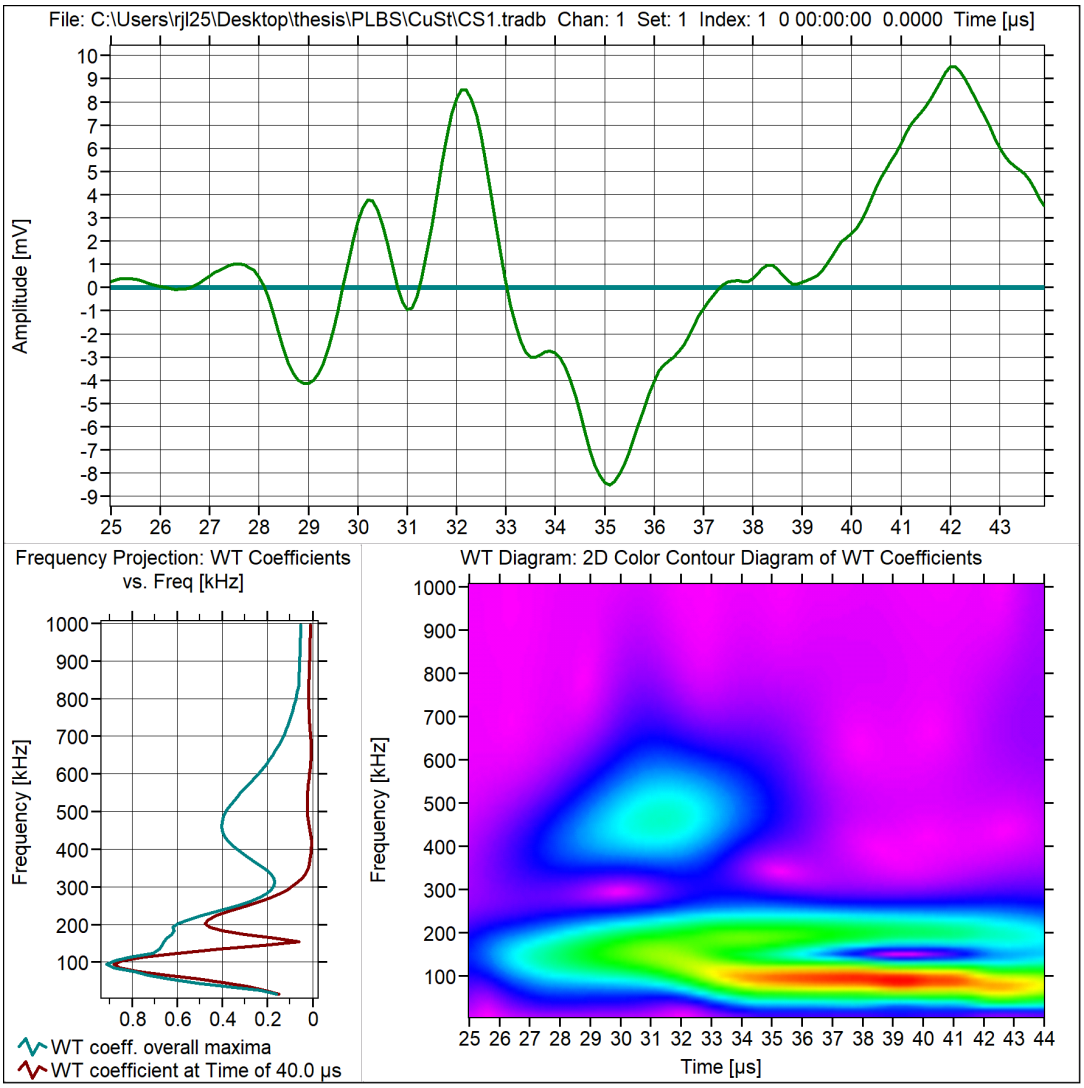


Figure 4.20: Wavelet Transform of undamaged Copper/Steel waveform at 40 microseconds.

The wavespeed was 2.50 km/s and the peak frequencies were 100 kHz and 200 kHz. These frequencies correspond to the first order mode that starts at the 0 km/s in Figure 4.5. This

mode was similar to one identified in Figure 4.19 in that comparing it to A0 mode in Figure 4.3 this mode was quicker at both those frequencies. The Wavelet Transformation was then performed on the collected waveforms from the damaged side of the Copper plate. The first Wavelet transformation that was done was at 28 microseconds shown in Figure 4.21. It should also be noted that the arrival of this waveform to the transducer was much slower than that for the undamaged case similar to previous stacked metal plate case.

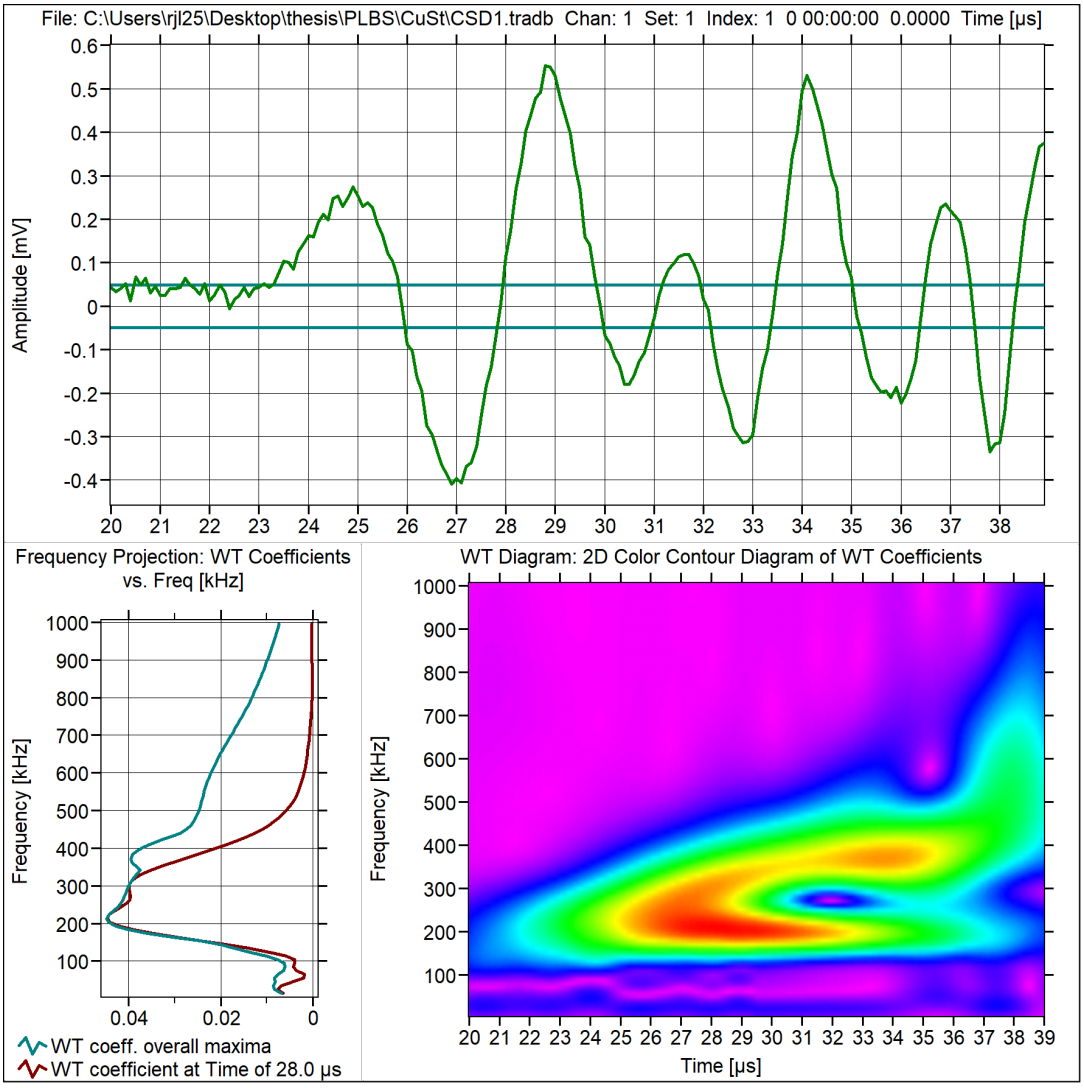


Figure 4.21: Wavelet Transform of damaged Copper/Steel waveform at 28 microseconds.

The wavespeed at this time was 3.57 km/s and had peak frequencies of 25 kHz, 200 kHz,

and 300 kHz. All of these frequencies corresponded to the S0 mode in Figure 4.3. As stated before, from the results of Figure 4.19 this mode is slower that its counterpart in Figure 4.5. The Wavelet Transformation was also done at the arrival of the flexural part of the waveform shown in Figure 4.22.

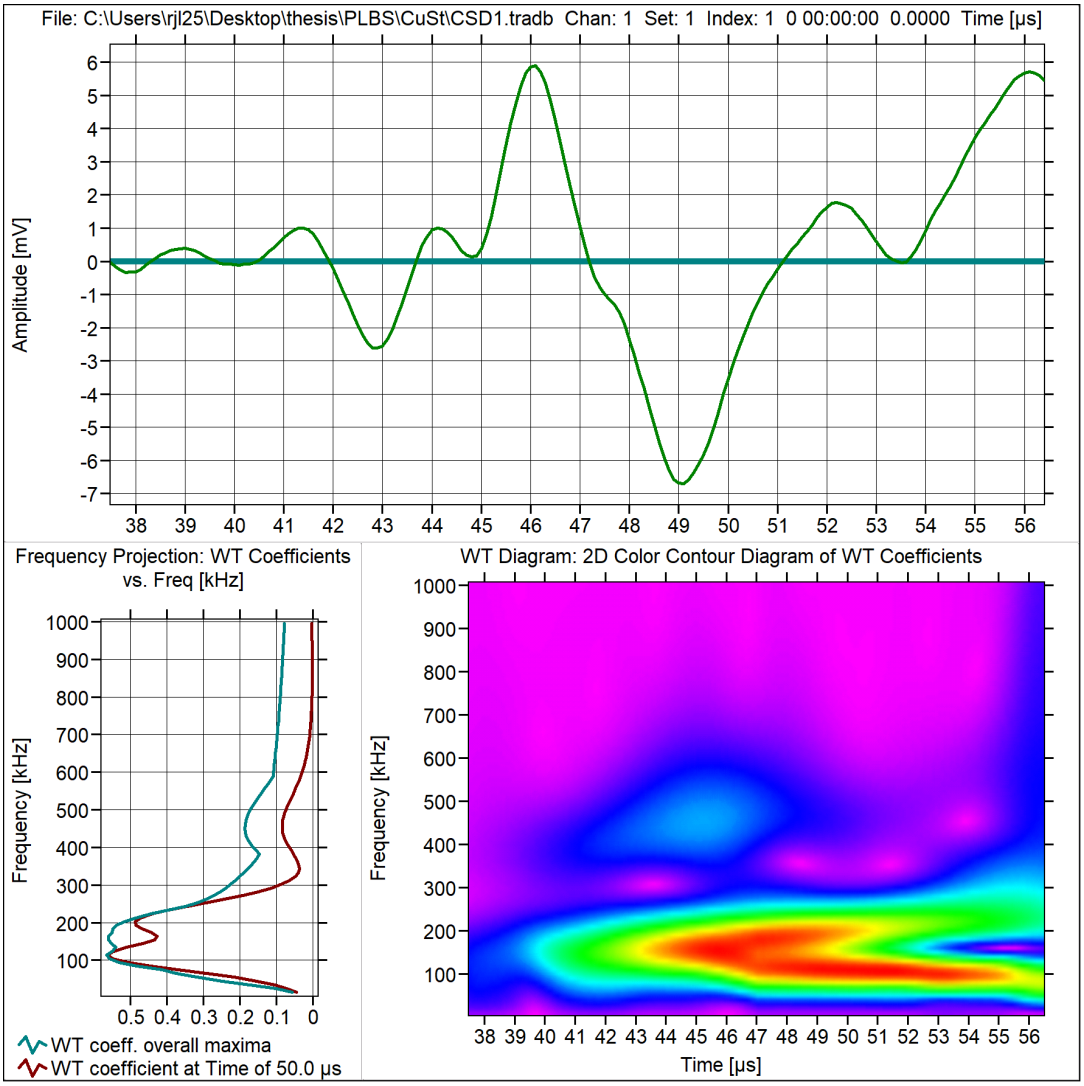


Figure 4.22: Wavelet Transform of damaged Copper/Steel waveform at 50 microseconds.

The speed of the wave was 2.00 km/s and had peak frequencies of 100 kHz, 200 kHz and 450 kHz. These frequencies roughly correspond to the A0 mode in Figure 4.3. Similar to the S0 mode the A0 modes speed is also slower at these frequencies.

Based on the results of the experiments for both cases, the one with Copper/Aluminum and Copper/Steel using a PLB and analyzing the wavespeed and frequency content can help identify a delamination. In both cases certain modes that were only present in the material system that has both plates stacked on top of each other were found. This was also true for the waveform over the embedded delamination region where only first order modes were excited by the PLB that had different characteristics then that of the both plates combined together. The ability to obtain promising results with isotropic materials suggests that this approach could be expanded to the carbon fiber.

# Chapter 5

# Laminated Carbon Fiber Reinforced Polymeric Matrix Composite Plate

## 5.1 Formulation of Governing Equations for Wave Speeds in Composite Plates

The composite material was assumed to be transversely isotropic because if the fibers are oriented in the x direction then the material properties are the same in the y and z direction but different in the x direction [1]. The governing equations for carbon fiber composites require five elastic constants whereas the isotropic materials only require two constants. The five material constants that were required were the Youngs modulus for the fiber direction and through thickness direction, Shear modulus for the fiber direction, and the Poissons ratio for the fiber and through thickness direction.

The composite material used to fabricate the composite panel was Hexcel T650-F854 [31]. The values for the five elastic constants for a single layer ply were previously determined in a study performed by Su and Ye [32]. A cross ply stacking sequence of $[0_2|90_3|0_2]$ was chosen to be studied as it greatly reduced the computational effort of using the transfer matrix method. A stiffness matrix was computed by taking the inverse of the compliance matrix

for each layer based on the fiber direction. A transformation matrix was used to adjust the stiffness matrix for a 90-degree rotation. The compliance matrix for a transversely isotropic material is stated in Equation 5.1 [1,22].

$$S = \begin{bmatrix} \frac{1}{E_1} & -\frac{\nu_{12}}{E_1} & -\frac{\nu_{12}}{E_1} & 0 & 0 & 0 \\ -\frac{\nu_{12}}{E_1} & \frac{1}{E_2} & -\frac{\nu_{23}}{E_2} & 0 & 0 & 0 \\ -\frac{\nu_{12}}{E_1} & -\frac{\nu_{23}}{E_2} & \frac{1}{E_2} & 0 & 0 & 0 \\ 0 & 0 & 0 & \frac{2(1+\nu_{23})}{E_2} & 0 & 0 \\ 0 & 0 & 0 & 0 & \frac{1}{G_{12}} & 0 \\ 0 & 0 & 0 & 0 & 0 & \frac{1}{G_{12}} \end{bmatrix} \tag{5.1}$$

The steps outlined in section 3 of the transfer matrix method were used to derive the dispersion relation for the composite plate. First, the dispersion relation was found for the whole stacking sequence using the Elastic constants $E_{11}$=153.67 GPa, $E_{22}$=9.49 GPa, $G_{12}$= 4.26 GPa, $\nu_{12}$=0.295, and $\nu_{23}$=0.381. The thickness of each ply was 0.038 cm. These values were input into the program (Appendix A) written to perform the transfer matrix method and dispersion curve for a stacking sequence of $[0_2|90_3|0_2]$ shown in Figure 5.1.

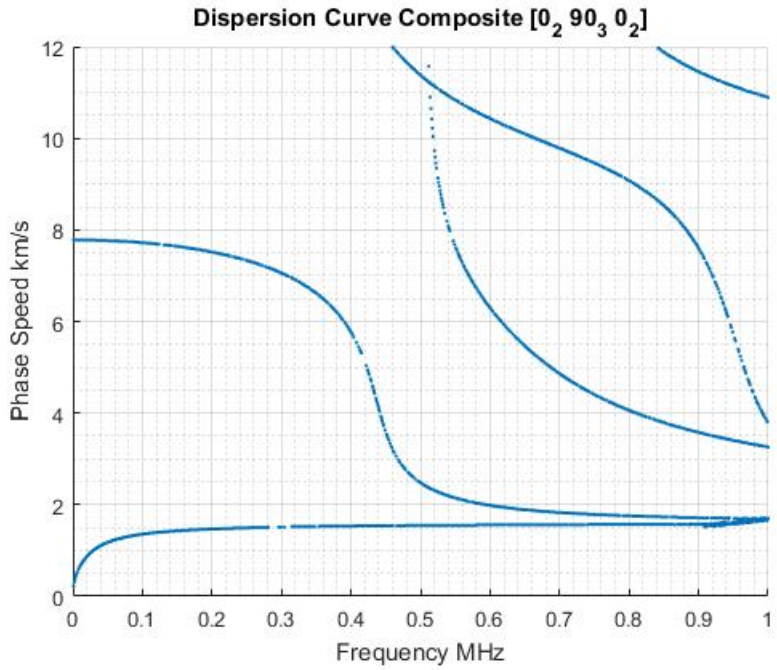


Figure 5.1: Dispersion Curves for Hexcel T650-F584 with a stacking sequence of $[0_2|90_3|0_2]$.

There were several plate modes that can propagate in the phase speed and frequency range. An interesting event occurs between 0.3 MHz and 0.6 MHz where there was a rapid decrease in the phase speeds of the mode that starts at close to 8 km/s which could be used to compare to the delamination dispersion curves.

Assuming a delamination creates a gap in between the first 0 and 90-degree layer then that zone would only be a $0_2$ composite. The same steps were followed as the whole stack sequence except a transformation of material properties doesn't need to be made as the plys were all the same direction. The dispersion curves for the $0_2$ composite is shown in Figure 5.2.

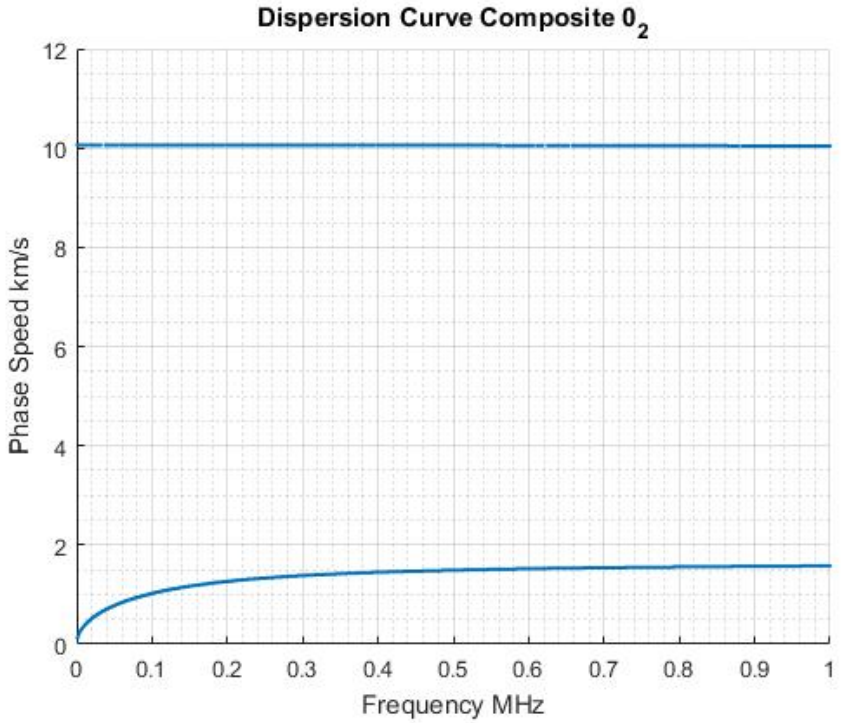


Figure 5.2: Dispersion Curves for Hexcel T650-F584 with a stacking sequence of $[0_2]$.

Unlike the dispersion curves for the whole carbon fiber laminate in Figure 5.1, the dispersion curves for the first two layers which are unidirectional resulted in only two modes that could propagate. The first mode that starts close to 0 km/s has a similar shape to that of the mode that occurs in the whole stack. However, the second mode that starts close to 10 km/s was different than any of the modes in the whole stack dispersion curve plot. This mode was also faster than the whole stack modes and if this mode could be excited by a PLB then this could be a key characteristic that identifies a delamination in the composite material.

## 5.2 Experimental Results in Composite Plates

A composite plate was fabricated to perform experiments. In order to keep the characteristic of the plate as similar as possible and not use multiple plates, it was decided that half of

the plate would be normal or undamaged and the other half would have the embedded delamination. A stacking sequence of $[0_2|90_3|0_2]$ using the Hexcel T650-F584 material was chosen. During the layup of the composite a Teflon sheet was placed in between the first 0 and 90 layer to create the embedded delamination. The composite was then placed in the autoclave to complete the manufacturing process. A picture of the composite with the embedded delamination is shown in Figure 5.3.

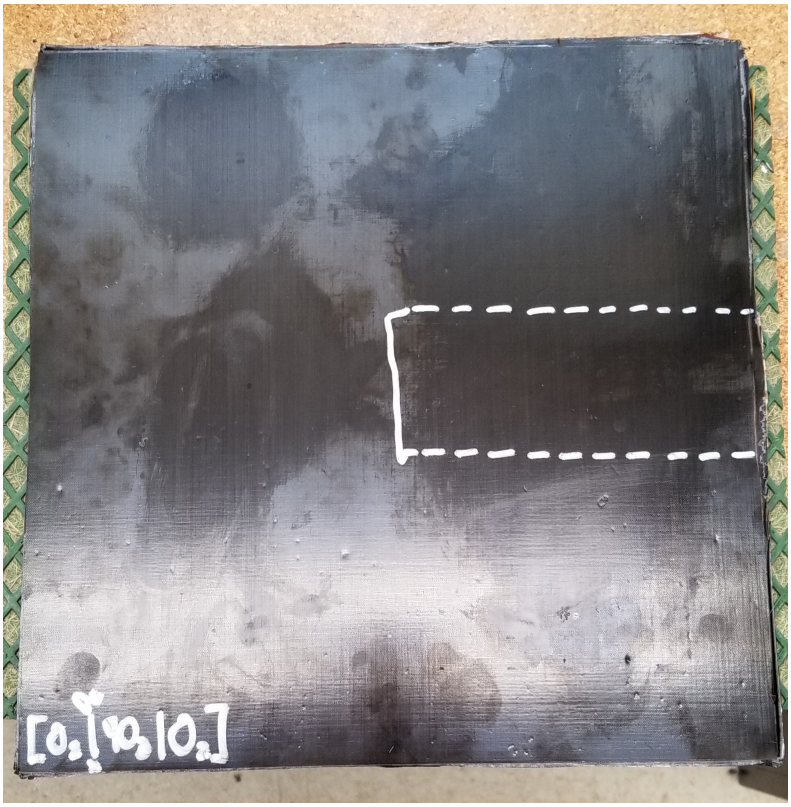

Figure 5.3: The finished $[0_2|90_3|0_2]$ composite with the region outlined by silver sharpie representing the embedded delamination.

A C scan was performed on the plate in the regions that would be used for PLBs. A picture demonstrating C scans being performed on the plate is shown in Figure 5.4. The results of the back surface reflection scans is shown in Figure 5.5 and 5.5, where 5.5 was the undamaged region of the composite and 5.6 was the embedded delamination region.

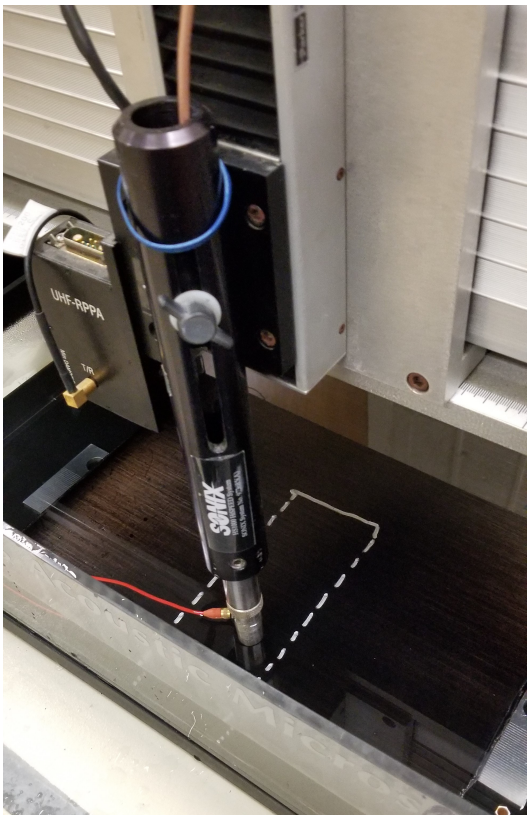


Figure 5.4: Image of the C scan being performed on the embedded delamination region of the plate.

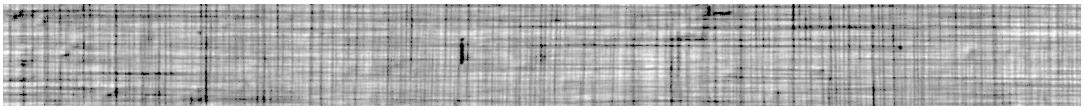

Figure 5.5: C scan image of the undamaged part of the plate.

Figure 5.6: C scan image of the embedded damage part of the part.

Both of these scans were back surface reflections C scan images and by comparing Figure 5.5 to 5.6 it can be seen that there is black box that appears in 5.6 that was not present in 5.5. This box was the embedded delamination region of the plate and the location for placing a transducer in order to collect the waveform over a delaminated region. These scans provide

evidence that the fabrication of the plate was correct and that the PLBs can be done in these areas to obtain the correct conditions.

After the scans were completed, the panel was placed on a rubber board and marked for the sensor location and PLB location. The SE1000 piezoelectric transducer was placed 10 cm away from an external trigger where the PLB would occur for both the undamaged and damaged side of the plate. A picture of the test setup is shown in Figure 5.7.

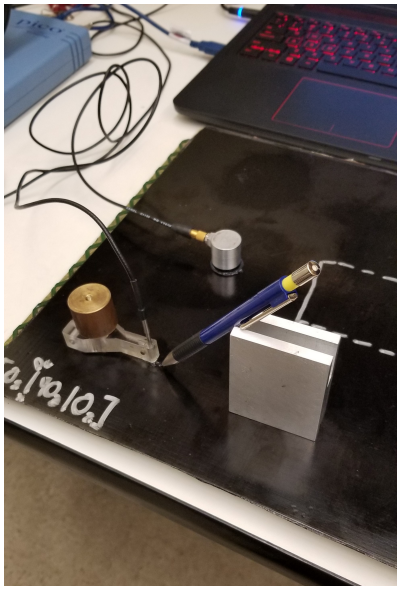

Figure 5.7: Composite Test Setup for perform PLBs 10 cm apart and collected the waveforms.

A 0.3 mm mechanical pencil with a lead length of 3mm was used to perform the PLB and a 3D printed block with a 3mm insert was used to ensure correct and reproducible pencil lead lengths. A total of 3 PLBs were performed at each location. A Picoscope was used to collect the waveforms. The settings for the data acquisition system were 10 Ms/s and 10k samples collected. Examples of a collected PLB waveforms from both sides of the plate is shown in Figure 5.8 and 5.9.

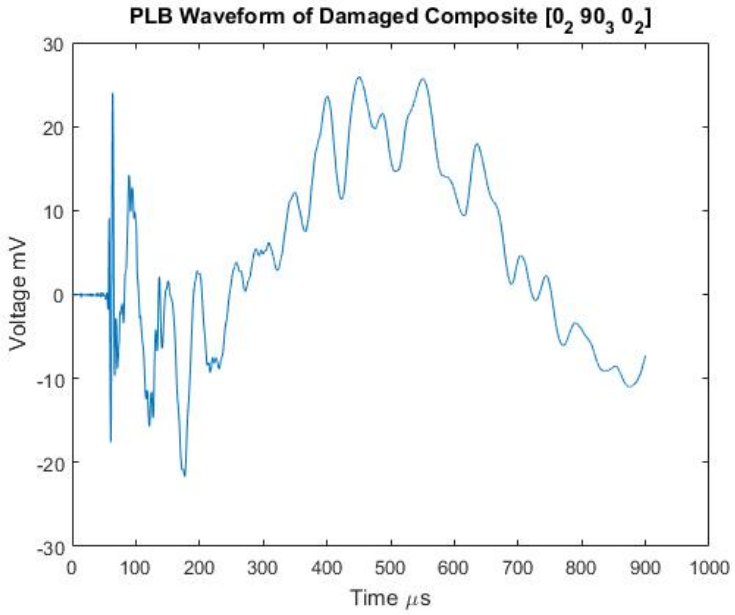


Figure 5.8: PLB waveform collected from the undamaged side of the composite plate.

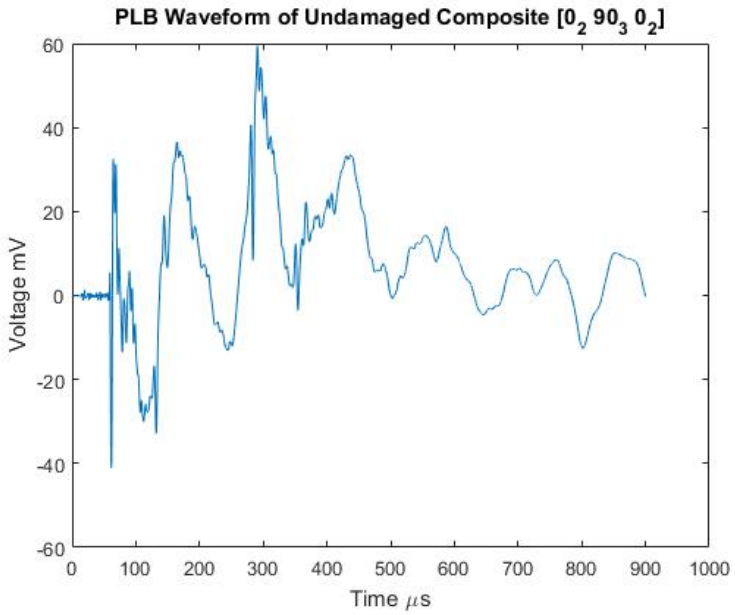


Figure 5.9: PLB waveform collected from the embedded delamination side of the composite plate.

Both the collected waveforms start from 0 seconds as an external trigger was used to trigger data collection as soon as the PLB had occured. The time of arrival of the waveform to the

transducer was close to that as described by the dispersion curves. The waveforms both had an extensional part that arrived first then a flexural part. After some time, constructive and destructive interference from the edges of the plate also appeared in the collected waveforms. This most likely wasn't the case for the extensional part but for the flexureal part this was a real possibility since the arrival of that part is close to the calculated arrival of a reflection form a surface.

A Fast Fourier Transform (FFT) was done on the entire signal collected for each PLB to see what frequencies were present in each version of the waveform. The FFT for the undamaged composite waveform is shown in Figure 5.10 and for the damaged composite is shown in Figure 5.11.

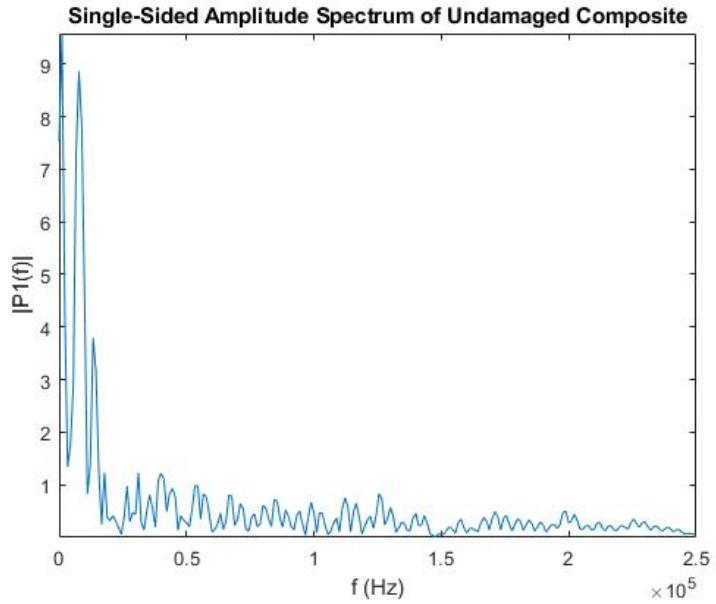


Figure 5.10: FFT of undamaged composite PLB waveform.

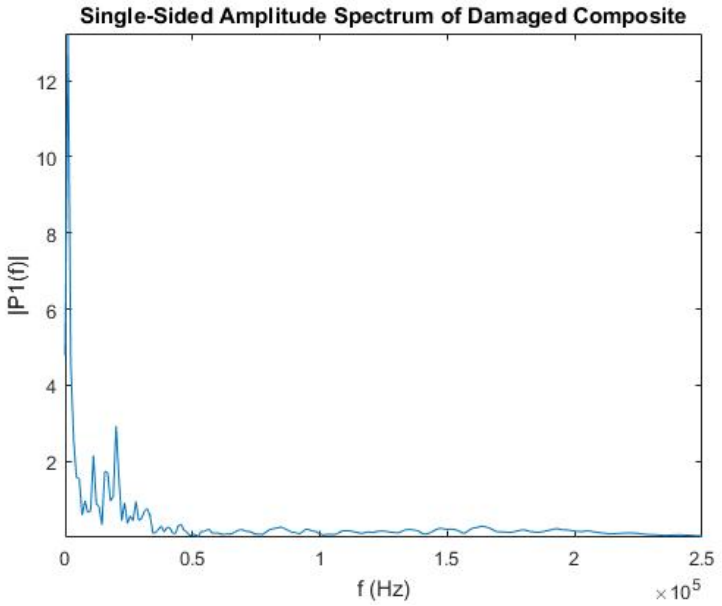


Figure 5.11: FFT of damaged composite PLB waveform.

It can be seen that the frequency spectrum for each case was different and that the undamaged case had a much broader frequency spectrum much like the dispersion curve to go with it. However, an FFT only gives the frequency spectrum not the time of arrival. A Wavelet Transforms gives both a frequency and time of arrival [30].

The collected waveforms were then converted to files that could be placed into Vallen Wavelet software. The extensional part of the undamaged waveform was first analyzed. Figure 5.12 and Figure 5.13 were the frequency spectrum at different time domains in the undamaged waveforms found using the Vallen Software.

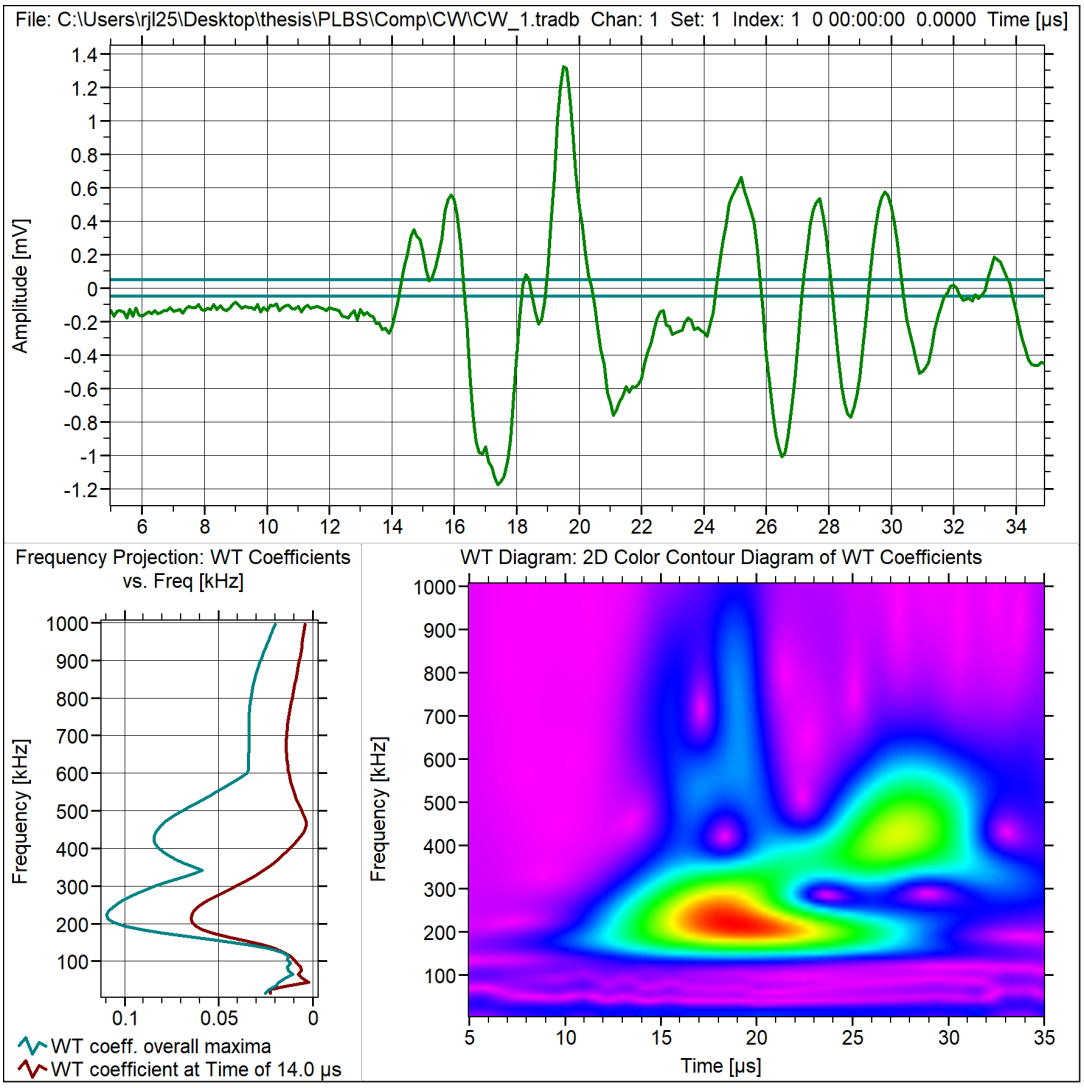


Figure 5.12: Wavelet Transform of the extensional part of the undamaged waveform frequency spectrum at 14 microseconds.

The PLB location and the transducer were 10 cm apart so the speed of the wave at this point in time was 7.14 km/s. The peak frequency that was present at the time was 215 kHz. Referencing Figure 5.1 of the dispersion curve of the complete stack for the composite plate that frequency corresponded to the mode starting at 7.75 km/s.

In Figure 5.13 the speed of the wave at this point in waveform was 3.57 km/s. There were a lot of peak frequencies that occur at that point in time. However, the peak frequency of

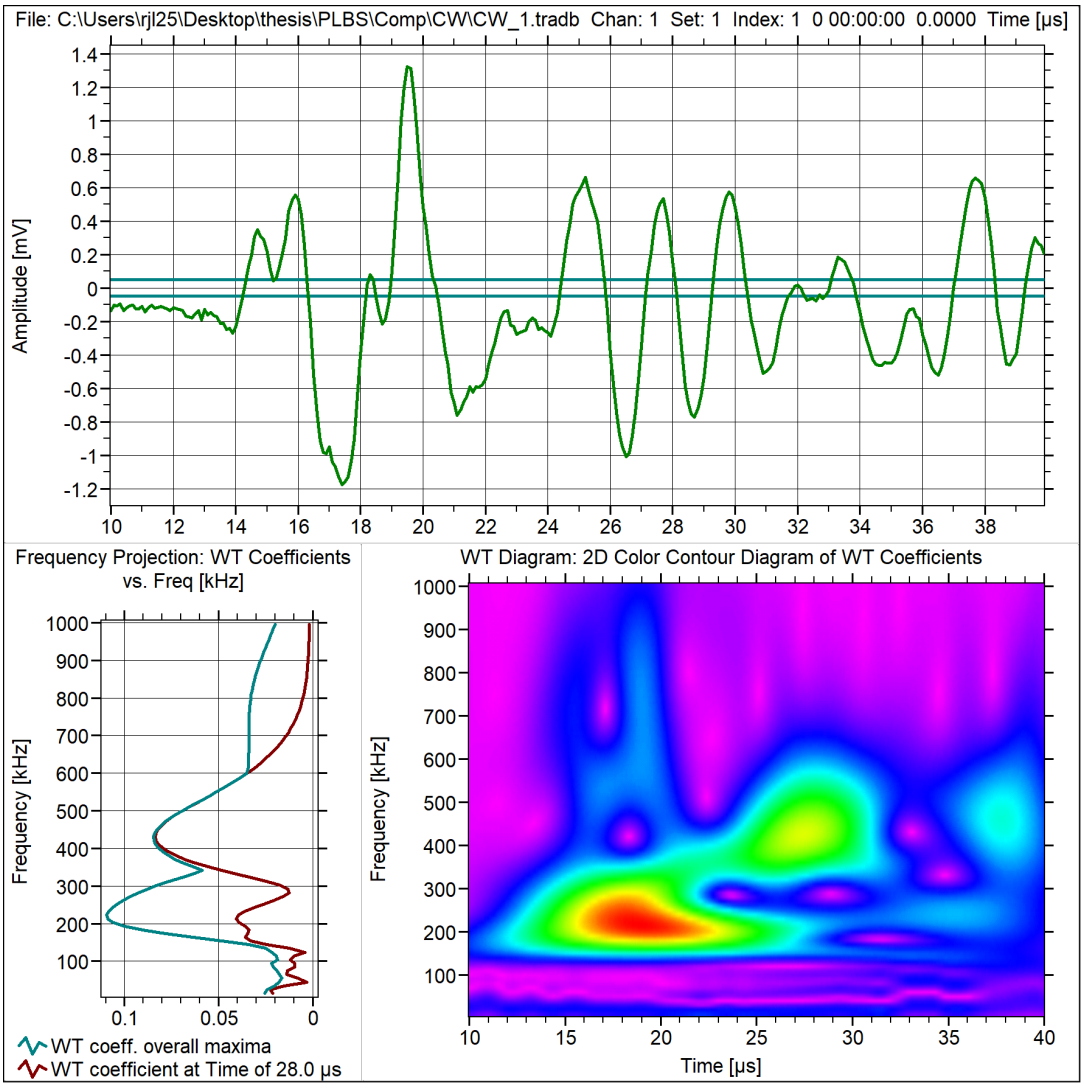


Figure 5.13: Wavelet Transform of the extensional part of the undamaged waveform frequency spectrum at 28 microseconds.

450 kHz also corresponded to the mode found in Figure 5.12 but at a lower speed and higher frequency. This was important because if you compare the dispersion curves for the whole stack (Figure 5.1) to dispersion curve for the first two layers (Figure 5.2) the modes between 400 and 500 kHz were not present in the first two layers at this wavespeed.

In Figure 5.2 the mode that starts at around 10 km/s was faster than that of any of the modes in the whole stack. Therefore, the wave should arrive earlier in time if there was a

delamination. A Wavelet Transformation was done on the extensional part of the wave form for the damaged case and the results of that is shown in Figure 5.14.

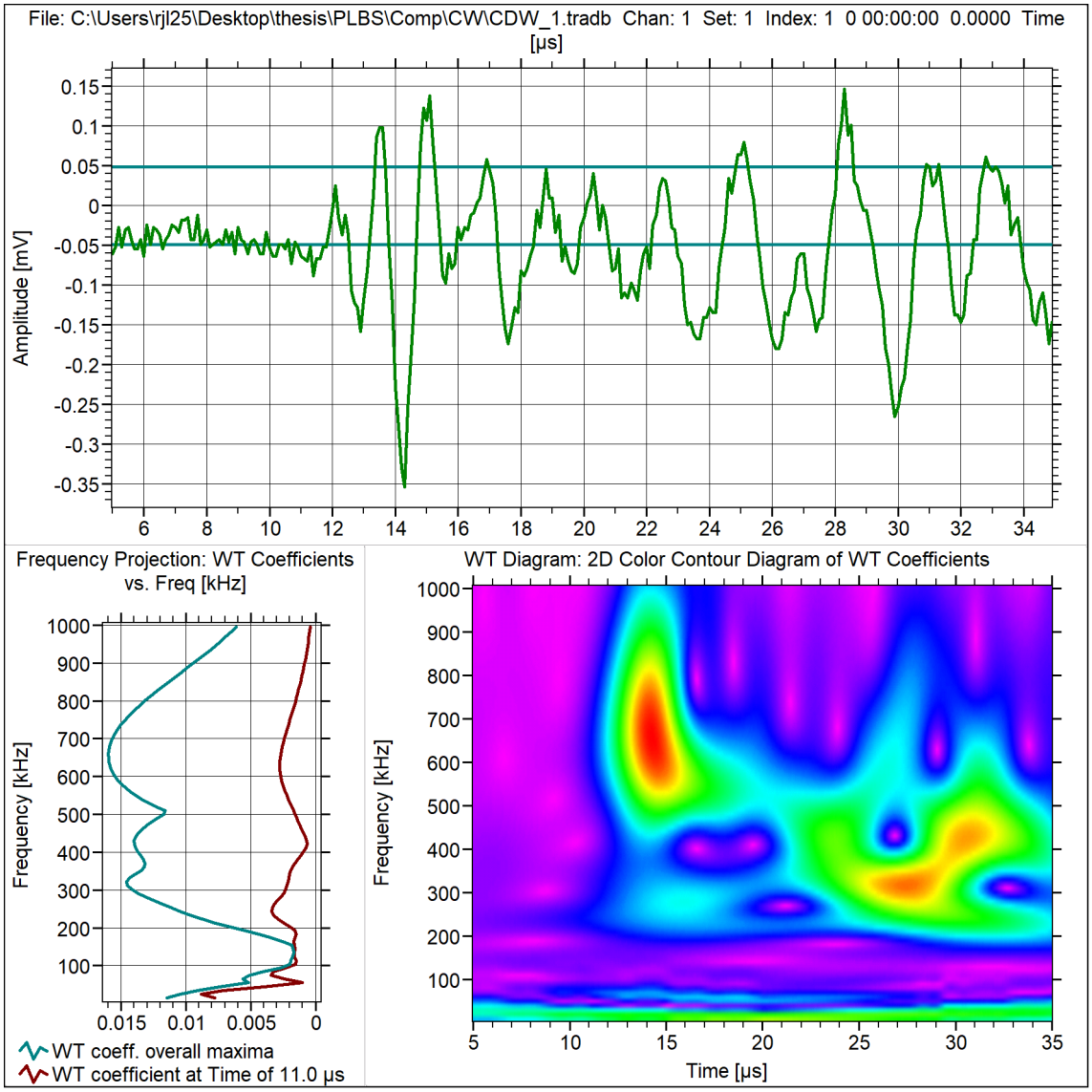


Figure 5.14: Wavelet Transform of the extensional part of the undamaged waveform frequency spectrum at 11 microseconds.

The frequency spectrum of the Wavelet Transformation at 11 microseconds had peak frequencies of 650 kHz, 250 kHz, 75 kHz, and 25 kHz. The arrival of the wave at 11 microseconds from 10 cm away has a wavespeed of 9.09 km/s. While this was not exact to the high-speed

mode in Figure 5.2. It does prove that there was a fast-moving wave that was not present in the undamaged case. The discrepancy may be due to the delaminated layers not being fully separated and some of the signal is allowed to pass through the gap between the layers. Evidence of this can be seen around 28 microseconds with possibly higher order modes being excited similar to the undamaged case but it was not as clear.

In Figure 5.1 and 5.2 the modes that start close to zero are roughly the same except for the mode in the damaged case was slightly quicker. An effort was made to see if they could be identified as they both appear in the dispersion curves in those figures. The arrival of the flexural part of the waveform for the undamaged waveform was the first to have the Wavelet Transformation performed. The results of which can be seen in Figure 5.15. When looking at the flexural part it was important to remember that this late in the time domain of the waveform it was possible for constructive and destructive inference to have taken place and affect the results of frequency spectrum. This meant that for the best results when trying to identify modes only the arrival of the flexural part was examined.

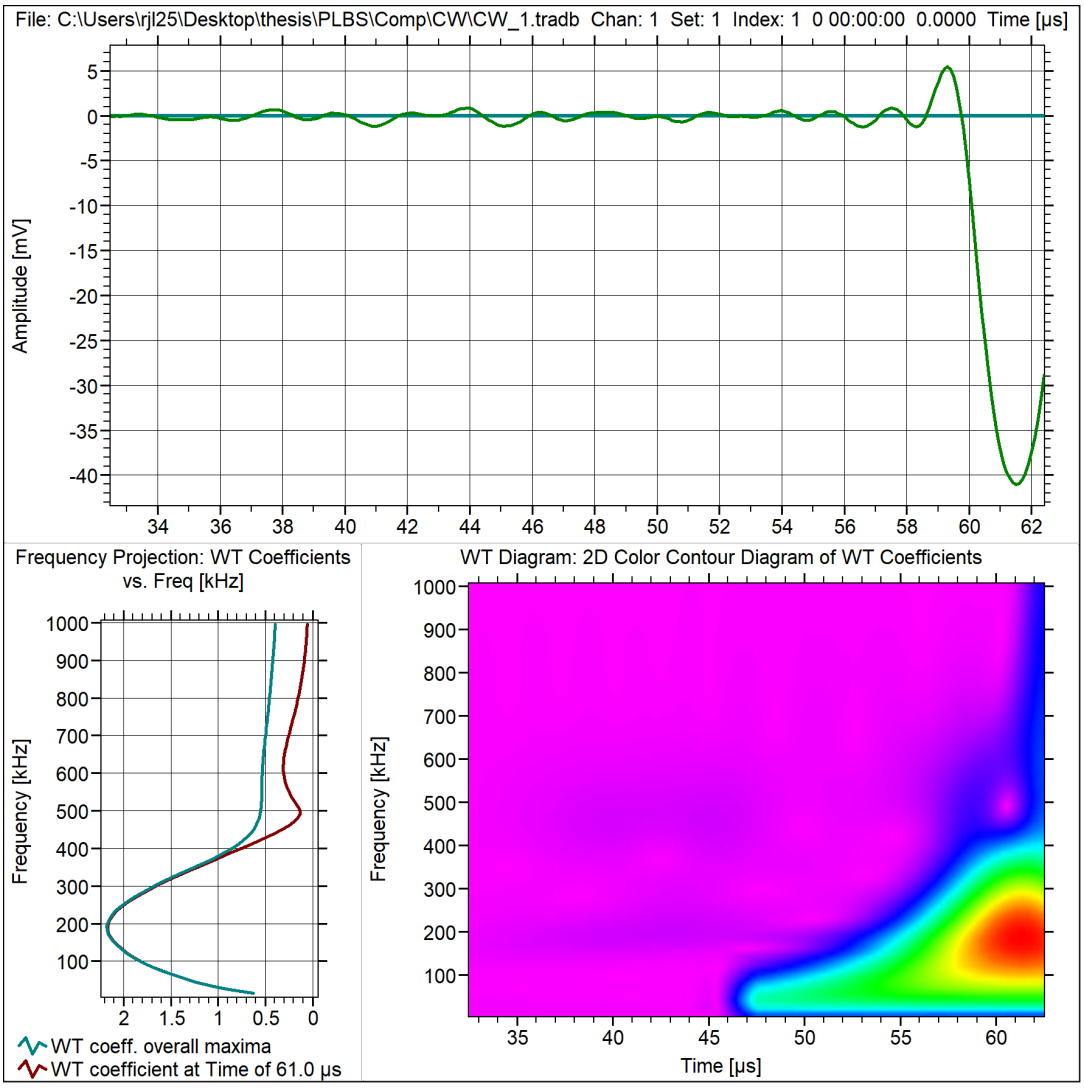


Figure 5.15: Wavelet Transform of the arrival of flexural part of the undamaged waveform frequency spectrum at 61 microseconds.

The waves speed at this point in time was 1.64 km/s and with a peak frequency of 200 kHz. In Figure 5.1 this would roughly correspond to the mode that starts at zero km/s. Next, the arrival of the flexural part of the waveform for the damaged waveform had a Wavelet Transformation performed. The results are shown in Figure 5.16.

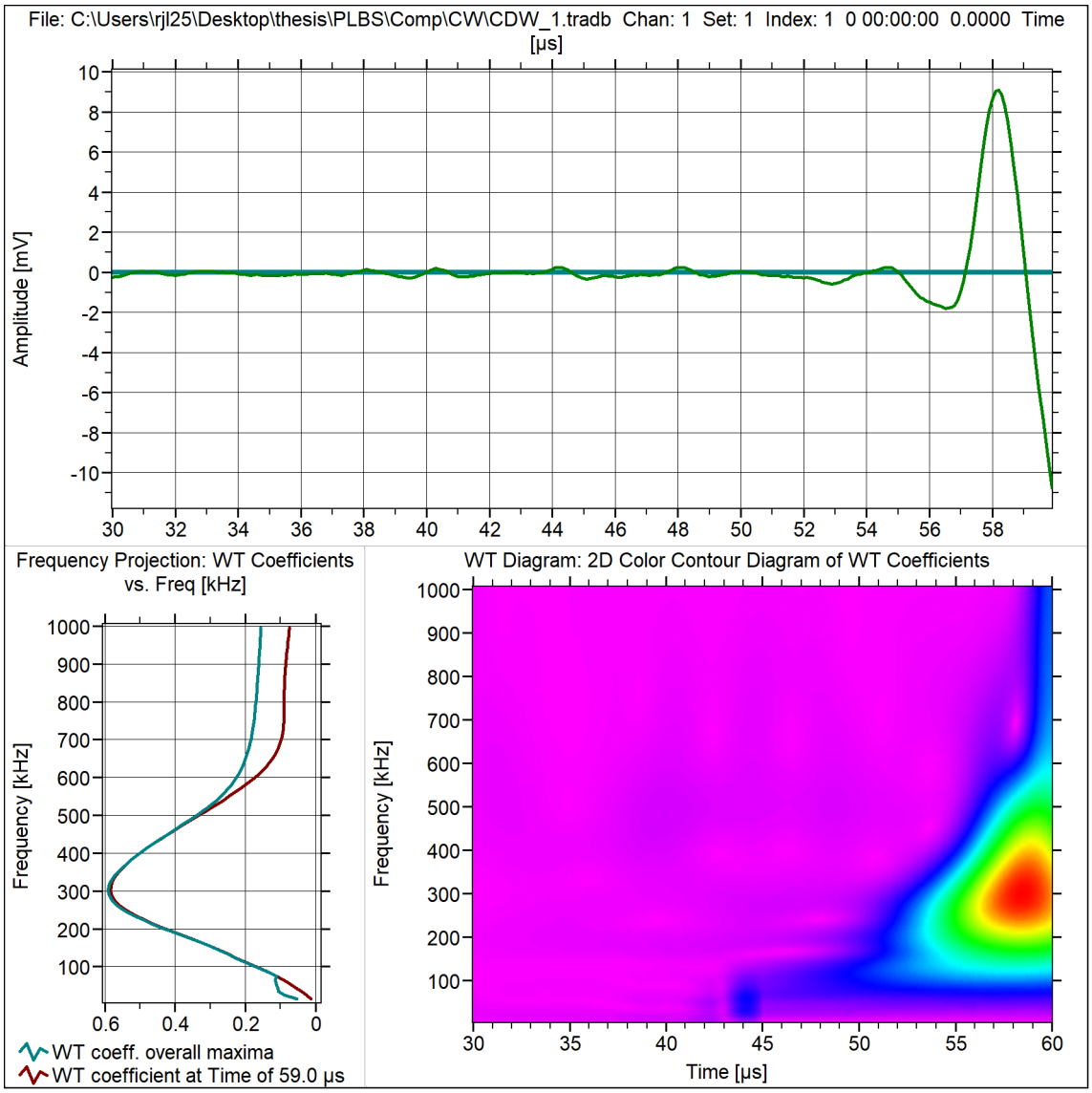


Figure 5.16: Wavelet Transform of the arrival of flexural part of the damaged waveform frequency spectrum at 59 microseconds.

The wave speed was 1.7 km/s which was slightly faster than that of the undamaged case. The frequency of wave was also higher. When compared to Figure 5.2 this frequency and wave speed corresponded also to the mode starting at 0 km/s.

The idea that a delamination can be found in a composite specimen just by the frequency and wave speed of a collected wave form is supported by the experiments. When looking at the

dispersion curves for when the plate is damaged vs undamaged there is a clear difference in the modes that can propagate in the specimen. When looking at experimental data there was evidence that also supported this theory. When an FFT was done on the collected waveforms for both cases the frequency spectrums were continuously different when comparing each case to each other. When Wavelet Transformations were performed on the data it was possible to identify certain wave modes that had a distinct difference between cases. One example was for the undamaged case it was found that the mode between 400-500 kHz had been excited by the PLB which was theoretically not possible in the damaged case. When this point was looked at the damaged case it was not clearly present. Also, the fast traveling mode in the damaged case as predicted by the dispersion curves was not present in the undamaged case. These key differences help prove that a delamination can be identified by exciting different wave modes that are not present in either the damaged or undamaged case.

# Chapter 6

# Conclusion

The results for both the isotropic plates and carbon fiber plate demonstrate that a delamination could be detected by examining the wavespeed and frequencies present in collected waveforms excited by PLBs. In both cases, distinct modes were able to be identified and of the ones identified it was clear that they were different or nonexistent in the opposing case being either undamaged or damaged. The ability to excite more than one wave mode also aided in the effort to demonstrate that a delamination could be detected. At times the wavespeeds and frequencies were not exact and could possibly be due to the step sized picked for the root solving method of the dispersion relations. However, they were close enough to enable the identification of a distinct mode. In the end the results of the experiments coincide with the dispersion curves for each material system in helping to identify certain modes that lead to concluding that a delamination was present.

# Chapter 7

# Future Work

In the future, the approach suggested in this study should be expanded to not only cross ply laminates but any layup with differing fiber directions. Also, the depth of the delamination should be taken into account as well as the separation between the layers in a delaminated region. Lastly, another type of damage should be studied that focuses on the stiffness reduction caused by matrix cracks.

# Bibliography


[1] M. Hyer and S. White, *Stress analysis of fiber-reinforced composite materials*. Lancaster, PA: DEStech Publications, 2009.

[2] C. Zweben, "Composite materials," in *Mechanical Engineers' Handbook*, M. Kutz, Ed., 2006, ch. 10, pp. 401–438.

[3] M. Kalanchiam and C. Chinnasamy, "Advantages of composite materials in aircraft structures," *International Journal of Aerospace and Mechanical Engineering*, vol. 6, no. 11, pp. 2428–2432, 2012.

[4] J. L. Rose, *Ultrasonic Guided Waves in Solid Media*. Cambridge University Press, 2014.

[5] D. Alleyne and P. Cawley, "The interaction of lamb waves with defects," *IEEE Transactions on Ultrasonics, Ferroelectrics and Frequency Control*, vol. 39, no. 3, pp. 381–397, 1992.

[6] S. Kessler, S. Spearing, and C. Soutis, "Damage detection in composite materials using lamb wave methods," *Smart Materials and Structures*, vol. 11, no. 2, pp. 269–278, 2002.

[7] M. Wisnom, "The role of delamination in failure of fibre-reinforced composites," *Philosophical Transactions of the Royal Society A: Mathematical, Physical and Engineering Sciences*, vol. 370, no. 1965, pp. 1850–1870, 2012.

[8] N. Guo and P. Cawley, "The interaction of lamb waves with delaminations in composite laminates," *The Journal of the Acoustical Society of America*, vol. 94, no. 4, pp. 2240–2246, 1993.

[9] N. Guo and P. Cawley, "Lamb wave reflection for the quick nondestructive evaluation of large composite laminates," *Materials Evaluation*, vol. 52, no. 3, 1994.

[10] N. Toyama and J. Takatsubo, "Lamb wave method for quick inspection of impact-induced delamination in composite laminates," *Composites Science and Technology*, vol. 64, no. 9, pp. 1293–1300, 2004.

[11] G. Petculescu, S. Krishnaswamy, and J. Achenbach, "Group delay measurements using modally selective lamb wave transducers for detection and sizing of delaminations in composites," *Smart Materials and Structures*, vol. 17, no. 1, 2007.

[12] C. Ramadas, M. J. Padiyar, K. Balasubramaniam, M. Joshi, and C. Krishnamurthy, "Delamination size detection using time of flight of anti-symmetric (ao) and mode converted ao mode of guided lamb waves," *Journal of Intelligent Material Systems and Structures*, vol. 21, no. 8, pp. 817–825, 2010.

[13] C. Yeum, J. I. H. Sohn, and H. Lim, "Instantaneous delamination detection in a composite plate using a dual piezoelectric transducer network," *Composite Structures*, vol. 94, no. 12, pp. 3490–3499, 2012.

[14] W. Staszewski, C. Boller, and G. Tomlinson, *Health Monitoring of Aerospace Structures*. New York, NY: Wiley and Sons, 2004.

[15] A. Shelke, T. Kundu, U. Amjad, K. Hahn, and W. Grill, "Mode-selective excitation and detection of ultrasonic guided waves for delamination detection in laminated aluminum plates," *IEEE Transactions on Ultrasonics, Ferroelectrics and Frequency Control*, vol. 58, no. 3, pp. 597–577, 2011.

[16] Z. Tian, L. Yu, and C. Leckey, "Delamination detection and quantification on laminated

composite structures with lamb waves and wavenumber analysis," *Journal of Intelligent Material Systems and Structures*, vol. 26, no. 13, pp. 1723–1738, 2015.

[17] ASTM. (2018, Aug.) Standard guide for determining the reproducibility of acoustic emission sensor response. [Online]. Available: https://www.astm.org/Standards/E976.htm

[18] M. Sause, "Investigation of pencil-lead breaks as acoustic emission sources," *Journal of Acoustic Emission*, vol. 29, 2011.

[19] C. Grosse. (2002, Sept) Hsu-nielsen source. [Online]. Available: https://www.ndt.net/ndtaz/content.php?id=474

[20] W. Thomson, "Transmission of elastic waves through a stratified solid medium," *Journal of Applied Physics*, vol. 21, no. 2, pp. 89–93, 1950.

[21] N. Haskell, "The dispersion of surface waves on multilayered media," *Bulletin of the Seismological Society of America*, vol. 43, no. 1, pp. 17–34, 1953.

[22] A. Nayfeh, "The general problem of elastic wave propagation in multilayered anisotropic media," *The Journal of the Acoustical Society of America*, vol. 89, no. 4, pp. 1521–1531, 1991.

[23] A. Maghsoodi, A. Ohadi, and M. Sadighi, "Calculation of wave dispersion curves in multilayered composite-metal plates," *Shock and Vibration*, pp. 1–6, 2014.

[24] D. Barazanchy and V. Giurgiutiu, "A unified formulation for predictive modeling of guided-ultrasonic wave dispersion curves in metallic and composite materials," *Journal of Intelligent Material Systems and Structures*, vol. 28, no. 10, pp. 1272–1286, 2016.

[25] ASM. (2018, Aug) Aluminum 6061-t6; 6061-t651. [Online]. Available: http://asm.matweb.com/search/SpecificMaterial.asp?bassnum=ma6061t6

[26] ASM. (2018, Aug) Aisi 4130 steel. [Online]. Available: http://asm.matweb.com/search/SpecificMaterial.asp?bassnum=m4130r

[27] MatWeb. (2018, Aug) Eagle brass 110 ept copper. [Online]. Available: http://www.matweb.com/search/datasheettext.aspx?matguid=eec7c85449024e8eba9c4d9ea47f3da2

[28] A. Metals and F. Group. (2018, Aug) Aisi 4130. [Online]. Available: https://www.steelforge.com/alloy-steel-4130-aisi-4130/

[29] C. Metals. (2018, Aug) Copper alloy 110. [Online]. Available: https://www.cometmetals.com/metal-detail?met_id=6386&product_txt=copper&pg_id=5143

[30] V. Systeme. (2018, Aug) Wavelet. [Online]. Available: http://www.vallen.de/products/software/

[31] Hexcel. (2018, Aug) Hexply f584. [Online]. Available: https://www.hexcel.com/user_area/content_media/raw/HexPly_F584_us_DataSheet.pdf

[32] Z. Su and L. Ye, "Lamb wave-based quantitative identification of delamination in cf/ep composite structures using artificial neural algorithm," *Composite Structures*, vol. 66, no. 1-4, pp. 627–637, 2004.

# Appendices

# Appendix A

# Dispersion Curve Code

## A.1 Main Program

```
% Cross ply Composite Dispersion Code
% Written by Ryan J Lane

clear all
close all
warning('off','MATLAB:illConditionedMatrix')
d1=0.38*2;
d2=0.38*3;

n=2;
m=1;
DA(1)=1;
Ang(1)=45;
for f=.00100:.00100:1.0000
 for c=.01:.0100:12.0

CT0=CCmat(0);
CB9=CCmat(pi/2);
```

```
19
20 [W1A,W3A,D11A,D13A,D21A,D23A,a1A,a3A]=WDC(CT0,1.528,c,f);
21 [W1S,W3S,D11S,D13S,D21S,D23S,a1S,a3S]=WDC(CB9,1.528,c,f);
22
23 [TA,T1A,T2A]=Tmat(W1A,W3A,D11A,D13A,D21A,D23A,f,c,d1,a1A,a3A);
24 [TS,T1S,T2S]=Tmat(W1S,W3S,D11S,D13S,D21S,D23S,f,c,d2,a1S,a3S);
25
26 T=TA*TS*TA;
27
28 A(1,1)=T(3,1);
29 A(1,2)=T(3,2);
30 A(2,1)=T(4,1);
31 A(2,2)=T(4,2);
32
33 DA(n)=det(A);
34
35 Ang(n)=wrapTo360(rad2deg(angle(DA(n))));
36
37 del(n)=abs(Ang(n)-Ang(n-1));
38 a(n)=180.0-mod(Ang(n-1),90.0);
39 b(n)=270.0-mod(Ang(n-1),90.0);
40
41 error=1.65*f+0.05;
42 if a(n)<=del(n) && del(n)<=b(n) && c~=0.01 && c>=error
43     RC(m)=c;
44     RF(m)=f;
45     m=m+1;
```

```
end
 n=n+1;
end

 end

scatter(RF,RC,3,'filled')
title('Dispersion Curve Composite [0_2 90_3 0_2]')
xlabel('Frequency MHz')
ylabel('Phase Speed km/s')
grid on
grid minor
axis([0,1,0,12])
```

## A.2 Stiffness Matrix Program

```
function [C]=CCmat(th)

Cp(1,1)=156.3855;
Cp(1,2)=4.6026;
Cp(1,3)=4.6026;
Cp(1,4)=0;
Cp(1,5)=0;
Cp(1,6)=0;
Cp(2,1)=4.6026;
Cp(2,2)=11.2370;
```

```
11 Cp(2,3)=4.3651;
12 Cp(2,4)=0;
13 Cp(2,5)=0;
14 Cp(2,6)=0;
15 Cp(3,1)=4.6026;
16 Cp(3,2)=4.3651;
17 Cp(3,3)=11.2370;
18 Cp(3,4)=0;
19 Cp(3,5)=0;
20 Cp(3,6)=0;
21 Cp(4,1)=0;
22 Cp(4,2)=0;
23 Cp(4,3)=0;
24 Cp(4,4)=3.44;
25 Cp(4,5)=0;
26 Cp(4,6)=0;
27 Cp(5,1)=0;
28 Cp(5,2)=0;
29 Cp(5,3)=0;
30 Cp(5,4)=0;
31 Cp(5,5)=4.26;
32 Cp(5,6)=0;
33 Cp(6,1)=0;
34 Cp(6,2)=0;
35 Cp(6,3)=0;
36 Cp(6,4)=0;
37 Cp(6,5)=0;
```

```
38 Cp(6,6)=4.26;
39
40 C(1,1)=Cp(1,1)*cos(th)^4+Cp(2,2)*sin(th)^4;
41 C(1,2)=Cp(1,2)*(cos(th)^4+sin(th)^4);
42 C(1,3)=Cp(1,3)*cos(th)^2+Cp(2,3)*sin(th)^2;
43 C(1,4)=0;
44 C(1,5)=0;
45 C(1,6)=0;
46 C(2,1)=Cp(1,2)*(cos(th)^4+sin(th)^4);
47 C(2,2)=Cp(1,1)*sin(th)^4+Cp(2,2)*cos(th)^4;
48 C(2,3)=Cp(2,3)*cos(th)^2+Cp(1,3)*sin(th)^2;
49 C(2,4)=0;
50 C(2,5)=0;
51 C(2,6)=0;
52 C(3,1)=Cp(1,3)*cos(th)^2+Cp(2,3)*sin(th)^2;
53 C(3,2)=Cp(2,3)*cos(th)^2+Cp(1,3)*sin(th)^2;
54 C(3,3)=Cp(3,3);
55 C(3,4)=0;
56 C(3,5)=0;
57 C(3,6)=0;
58 C(4,1)=0;
59 C(4,2)=0;
60 C(4,3)=0;
61 C(4,4)=Cp(4,4)*cos(th)^2+Cp(5,5)*sin(th)^2;
62 C(4,5)=0;
63 C(4,6)=0;
64 C(5,1)=0;
```

```
65 C(5,2)=0;
66 C(5,3)=0;
67 C(5,4)=0;
68 C(5,5)=Cp(5,5)*cos(th)^2+Cp(4,4)*sin(th)^2;
69 C(5,6)=0;
70 Cp(6,1)=0;
71 Cp(6,2)=0;
72 Cp(6,3)=0;
73 Cp(6,4)=0;
74 Cp(6,5)=0;
75 C(6,6)=Cp(6,6)*(sin(th)^4+cos(th)^4);
76
77 end
```

## A.3 Displacement Ratio Program

```
1  function [W1,W3,D11,D13,D21,D23,a1,a3] = WDC(C,ro,c,f)
2
3  w=f*2*pi;
4  k=w/c;
5
6  % a1=sqrt(((ro*(c^2))/C(1,1))-1);
7  % a3=sqrt(((ro*(c^2))/C(5,5))-1);
8
9  A=C(3,3)*C(5,5);
10
```

```
11 B=(C(1,1)-ro*c^2)*C(3,3)+(C(5,5)-ro*c^2)*C(5,5)-(C(1,3)+C(5,5))^2;
12
13 C1=(C(1,1)-ro*c^2)*(C(5,5)-ro*c^2);
14
15 a1=sqrt((-B+sqrt(((B^2)-4*A*C1)))/(2*A));
16 a3=sqrt((-B-sqrt(((B^2)-4*A*C1)))/(2*A));
17 %
18 %
19 W1=(ro*(c^2)-C(1,1)-C(5,5)*a1^2)/((C(1,3)+C(5,5))*a1);
20 W3=(ro*(c^2)-C(1,1)-C(5,5)*a3^2)/((C(1,3)+C(5,5))*a3);
21
22 D11=1i*k*((C(1,3)+C(3,3)*a1*W1));
23 D13=1i*k*((C(1,3)+C(3,3)*a3*W3));
24
25 D21=1i*k*C(5,5)*(a1+W1);
26 D23=1i*k*C(5,5)*(a3+W3);
27
28 end
```

## A.4 Transfer Matrix Program

```
1 function [T,T1,T2] = Tmat(W1,W3,D11,D13,D21,D23,f,c,d,a1,a3)
2
3 w=f*2*pi;
4 k=w/c;
5 a2=-a1;
```

```
6  a4=-a3;
7
8  T1(1,1)=1;
9  T1(1,2)=1;
10 T1(1,3)=1;
11 T1(1,4)=1;
12 T1(2,1)=W1;
13 T1(2,2)=-W1;
14 T1(2,3)=W3;
15 T1(2,4)=-W3;
16 T1(3,1)=D11;
17 T1(3,2)=D11;
18 T1(3,3)=D13;
19 T1(3,4)=D13;
20 T1(4,1)=D21;
21 T1(4,2)=-D21;
22 T1(4,3)=D23;
23 T1(4,4)=-D23;
24
25 T2(1,1)=exp(1i*k*a1*d);
26 T2(1,2)=0;
27 T2(1,3)=0;
28 T2(1,4)=0;
29 T2(2,1)=0;
30 T2(2,2)=exp(1i*k*a2*d);
31 T2(2,3)=0;
32 T2(2,4)=0;
```

```
33 T2(3,1)=0;
34 T2(3,2)=0;
35 T2(3,3)=exp(1i*k*a3*d);
36 T2(3,4)=0;
37 T2(2,4)=0;
38 T2(4,1)=0;
39 T2(4,2)=0;
40 T2(4,3)=0;
41 T2(4,4)=exp(1i*k*a4*d);
42
43 T=T1*T2/(T1);
44
45 end
```